



Late Paleozoic evolution of the South Tien Shan: Insights from $P-T$ estimates and allanite geochronology on retrogressed eclogites (Chatkal range, Kyrgyzstan)

Chloé Loury^{a,*}, Yann Rolland^a, Bénédicte Cenki-Tok^b, Pierre Lanari^c, Stéphane Guillot^d

^a Géoazur, Observatoire de la Côte d'Azur, Université de Nice Sophia-Antipolis, 250 rue A. Einstein, 06560 Valbonne, France

^b Géosciences Montpellier, UMR 5243, Université Montpellier, Place Eugène Bataillon, 34095 Montpellier, France

^c Institute of Geological Sciences, University of Bern, Baltzerstrasse 1+3, CH3012 Bern, Switzerland

^d ISTerre, Université de Grenoble Alpes, CNRS, 1381 rue de la Piscine, 38041 Grenoble, France

ARTICLE INFO

Article history:

Received 26 February 2015

Received in revised form 27 May 2015

Accepted 17 June 2015

Available online 2 July 2015

Keywords:

South Tien Shan

Chatkal range

Metamorphic evolution

Micro-mapping

Allanite geochronology

ABSTRACT

In the South Tien Shan range (Kyrgyzstan), the Late Paleozoic geodynamic evolution remains debated especially to the west of the Talas-Fergana fault (TFF) fault where suture-related high-pressure (HP) rocks are scarce. We provide new petrological and geochronological data on garnet amphibolites from the Chatkal range, to the west of the TFF, northwest of the South Tien Shan suture. These rocks are retrogressed eclogites. We used a micro-mapping approach combined with forward modeling and empirical thermobarometry to decipher the $P-T$ path of these amphibolitized eclogites. The metamorphic peak conditions culminated at $490 \pm 50^\circ\text{C}$ and 18.5 ± 2 kbar and were followed by higher temperature retrogression ($\sim 560^\circ\text{C}$ at $11-7$ kbar). In order to constrain the age of the HP stage, we dated allanite crystals texturally coeval to the HP mineral assemblage. Allanite grains dated in situ with a U-Pb LA-ICPMS methodology yield an age of 301 ± 15 Ma. Compared with previously published data for the east of the TFF, these $P-T$ constraints allow improving the understanding of the Late Paleozoic geodynamic evolution of the South Tien Shan. To the east of TFF, the Turkestan Ocean closed around 320 Ma with the collision of the Tarim Craton with the Kazakh microcontinent. To the west of TFF, the Turkestan Ocean closed around 300 Ma, when the Alai block collided with the Kazakh microcontinent. This later collision involved nappe-stacking and intense subvertical folding in the western South Tien Shan. This complex folding explains the S-shape of the suture to the west of the TFF that cannot be observed in the eastern part. These new data allow us to propose a distinct tectonic evolution of the two sides of the TFF, which suggests that this fault was a major transform fault before being a strike-slip intra-continental fault.

© 2015 Elsevier Ltd. All rights reserved.

1. Introduction

The understanding of subduction, collision and accretion dynamics relies on the reconstruction of precise Pressure-Temperature ($P-T$) paths of high-pressure (HP) rocks having undergone a complete burial-exhumation cycle. Dating successive stages ($-t$) of the evolution of such rocks is essential to estimate the timing and rates of such mechanisms (Rubatto and Hermann, 2001). Constraining the age of the HP metamorphic peak in continental unit and the onset of exhumation is particularly important as it generally corresponds to the subduction-collision transition with continental subduction (Agard et al., 2009). If the

$P-T-t$ paths of HP rocks of the most studied collisional orogens, as the Alps or the Himalayas, are quite well constrained (e.g. Berger and Bousquet, 2008; Guillot et al., 2008), it is not the case for other accretionary orogens such as the Central Asia Orogenic Belt (CAOB) where a lack of petrochronological data prevents a good understanding of the geodynamic evolution of the area.

The CAOB results from multiple collages of Precambrian microcontinents, Paleozoic volcanic arcs, ophiolites and accretionary complex from the Neoproterozoic to the Late Paleozoic times (e.g. Windley et al., 2007; Xiao et al., 2013; Kröner et al., 2014). The most widely accepted accretion model for the CAOB is an archipelago-type model, similar to that of the circum-Pacific Mesozoic-Cenozoic accretionary orogens (Coleman, 1989; Jolivet et al., 1989; Filippova et al., 2001; Windley et al., 2007; Xiao et al., 2013; Rojas-Agramonte et al., 2014). During the late Carboniferous to Early Permian, these multiple accreted blocks, constituting

* Corresponding author.

E-mail address: chloe.loury@geoazur.unice.fr (C. Loury).

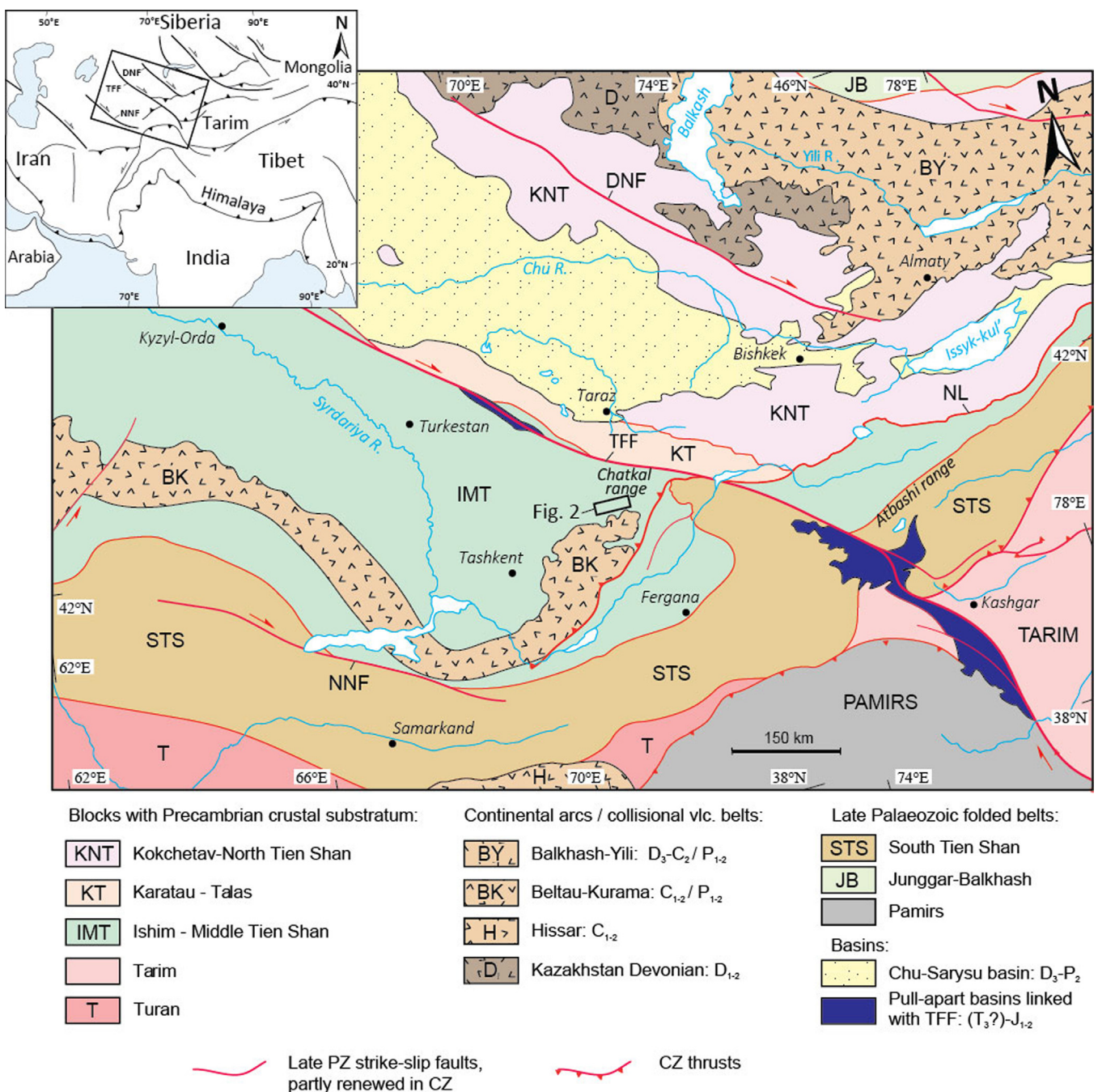


Fig. 1. (a) Location of map (b) in Central Asia. (b) Geotectonic map of the western Tien Shan and the southern Kazakhstan (late Mesozoic and Cenozoic cover removed) (modified after Rolland et al., 2013). The black box indicates location of Fig. 2. Abbreviations of faults names: TFF – Talas–Fergana, NNF – North Nuratau, DNF – Djalair–Naiman, NL – Nikolaev Line.

the Kazakh microcontinent, collided with the Siberia, Baltica, Tarim and Alai cratons (Filippova et al., 2001; Heubeck, 2001; Windley et al., 2007). The collision of the Tarim Craton and Alai microcontinent with the Kazakh continent led to the formation of the South Tien Shan fold-and-thrust belt during Late Carboniferous (e.g. Biske and Seltmann, 2010). From the Late Permian to the Early Mesozoic times, during the post-collisional evolution, the CAOB was affected by transcurrent tectonics along major ENE and NW striking strike-slip faults (Fig. 1) (e.g. Allen and Vincent, 1997; Laurent-Charvet et al., 2003; Wang et al., 2009, 2010). In the Tien Shan range, the largest of these faults, the Talas–Fergana fault (TFF), cross-cuts the south-western Kazakhstan and western Kyrgyzstan for over 2000 km (Burtman, 1964, 1980). The TFF was initiated in Late

Carboniferous and Permian times and was reactivated several times (Konopelko et al., 2013; Rolland et al., 2013 and references therein). It is currently reactivated due to the India-Asia collision since at least 10 Ma. Consequently, the structures formed prior to the fault activation, especially the South Tien Shan suture (STSs), between Middle Tien Shan and South Tien Shan, are offset on both sides of the fault (Fig. 1). It is therefore difficult to reconstruct the pre-Permian evolution of the Tien Shan and more particularly the last collisional event leading to the STSs formation.

To the east of the TFF, HP rocks are exposed along the STSs in the Atbashi range and in Chinese Western Tien Shan (Bakirov, 1978; Bakirov and Kotov, 1988; Tagiri et al., 1995; Gao and Klemd, 2003; Simonov et al., 2008; Hegner et al., 2010; Tian & Wei, 2013; Loury

et al., 2015). Petrological and geochronological data available for these rocks show a coherent Late Carboniferous P - T evolution with HP peak ranging from ca. 330–340 Ma in the east (Kekesu river, China) to ca. 320 Ma in the west (Atbashi range, Kyrgyzstan) and exhumation at the surface at ca. 300 Ma (e.g. Simonov et al., 2008; Hegner et al., 2010; Wang et al., 2010; Tian and Wei, 2013; Liu et al., 2014).

To the west of the TFF, relicts of oceanic rocks, such as serpentinites or gabbros, are exposed along the STSs (Burtman, 1975; Kristov and Mikolaichuk, 1983; Tursungaziev and Petrov, 2008; Alexeiev et al., 2015a,b). In this area there are no preserved HP rocks (similar to the eclogites found to the east of the TFF) exposed along the STSs. However, relicts of HP rocks are suspected in the Chatkal range (Bakirov et al., 2003), tens of kilometers west of the STSs (Fig. 1). However, only few structural data are available and the P - T - t history of such HP rocks remains unknown. The geodynamic history of this range is difficult to decipher as geochronological data for surrounding rocks are scarce and controversial (Bakirov et al., 1996; Rojas-Agramonte et al., 2014). In this study we provide new data on garnet amphibolite of the Chatkal range, which have been identified as strongly retrogressed eclogite. As they underwent subduction before collision their metamorphic history brings insights for the subduction and the following collision history of the Middle and the South Tien Shan blocks. To decipher the P - T path of these retrogressed HP rocks we used a micro-mapping approach which is particularly relevant for this kind of texturally complex rocks (Lanari et al., 2013). We obtained a P - T path from the HP peak to the late exhumation stages. This study was complemented by allanite U-Pb in situ LA-ICPMS dating to constrain the timing of the HP stage corresponding to the onset of exhumation. The obtained petrological and geochronological data can be combined to obtain a P - T - t path for the HP rocks of the Chatkal range. These new petrochronological data improve our understanding of the Chatkal range in the context of the CAOB and provide significant constraints for lateral correlations on both sides of the TFF.

2. Geological setting

2.1. General framework

The Tien Shan range constitutes the southwestern part of the CAOB (Fig. 1). It extends for 2500 km from Uzbekistan to the Xinjiang Province in western China. In Kyrgyzstan, the Tien Shan range is divided into three parts: the North Tien Shan (NTS), the Middle Tien Shan (MTS) and the South Tien Shan (STS) (Fig. 1). The NTS is made of two domains: the Kokchetav-North Tien Shan and the Karatau-Talas domain. The Kokchetav-North Tien Shan consists of Precambrian continental fragments, early Paleozoic island arcs, ophiolites and HP metamorphic complexes that were amalgamated prior to the Middle Ordovician (Mikolaichuk et al., 1997; Maksumova et al., 2001; Ghes, 2008; Alexeiev et al., 2011; Kröner et al., 2012). During Middle Ordovician to Early Silurian, this domain was intruded by a large volume of granitoids firstly in a continental arc setting and then in a collisional setting (Mikolaichuk et al., 1997; Maksumova et al., 2001; Konopelko et al., 2008; Degtyarev, 2012; De Grave et al., 2012; Kröner et al., 2014). The Karatau-Talas domain is mainly made of unmetamorphosed shallow marine and continental sediments of Neoproterozoic age, Cambrian to Ordovician carbonates, and of low-grade turbidites and shales probably Cambrian to Ordovician in age (Maksumova et al., 2001; Ghes, 2008; Tursungaziev and Petrov, 2008). The origin of the Karatau-Talas domain is debated: it could represent either the marginal part of the MTS (Kröner et al., 2013) or a microcontinent, between KNT and MTS (Maksumova et al., 2001).

The MTS represents the southern part of a 2000 km long Precambrian microcontinent, called the Ishim-Middle Tien Shan, which extends to the western part of northern Kazakhstan (Avdeev and Kovalev, 1989). It was accreted to the NTS during the Early Ordovician following the closure of the Terksey Ocean (Lomize et al., 1997; Mikolaichuk et al., 1997; Burtman, 2006). Detrital zircon ages suggest that the MTS was rifted from the Tarim, which itself derived from the northern margin of Gondwana (Rojas-Agramonte et al., 2014). The oldest rocks are gneisses and amphibolites exposed in the Kuilyu complex and dated at 2.4–1.8 Ga (Kiselev et al., 1993; Bakirov and Maksumova, 2001; Maksumova et al., 2001; Glorie et al., 2011). This basement is overlain by Neoproterozoic to Middle Ordovician sedimentary series, similar to those of the Tarim craton (Eganov and Sovietov, 1979; Osmontbetov, 1982; Maksumova et al., 2001; Tursungaziev & Petrov, 2008). From the Late Ordovician to the Upper Carboniferous, thick sedimentary series mainly made of carbonates were deposited (e.g. Maksumova et al., 2001; Alexeiev et al., 2015a,b). In the Chatkal range, the southwestern part of the MTS is characterized by arc-related magmatic rocks cross-cutting this sedimentary cover and by a metamorphic complex (e.g. Biske, 1996; Seliverstov and Ghes, 2001; Filippova et al., 2001; Bakirov et al., 2003; Alexeiev et al., 2009a; Seltmann et al., 2011).

The STS is a fold-and-thrust belt formed during the Late Paleozoic. It is mainly composed of Silurian to Late Paleozoic marine deposits as well as oceanic and continental eclogites and ophiolites exhumed along top-to-the-north thrusts (Bakirov, 1978; Bakirov and Kotov, 1988; Loury et al., 2015; Jourdon et al., this volume). The STS resulted from the Late Carboniferous collision of the early Paleozoic Kazakhstan microcontinent to the north with the Alai block and Tarim craton to the south-west and south-east respectively (e.g. Biske, 1995, 1996; Filippova et al., 2001). The polarity of the subduction leading to this collision is debated: either south-directed (e.g. Wang et al., 2008; Charvet et al., 2011; Loury et al., 2015) or north-directed (e.g. Windley et al., 1990; Biske, 1996; Makarov et al., 2010). Another model, with two antithetic subductions under the Kazakhstan microcontinent and under the Tarim, is also proposed (Ge et al., 2012; Alexeiev et al., 2015a,b; Jourdon et al., this volume).

In western Kyrgyzstan, the Tien Shan range is cross-cut by the 2000 km long NW striking TFF. This fault is still active and has a long and complex history. Although the apparent slip is dextral (Fig. 1), some evidence for left-lateral displacement during the earliest phases of deformation is also documented (Galitskiy, 1967; Allen et al., 2001; Alexeiev et al., 2009a). The maximum total offset along this fault from its activation during the Late Carboniferous (c.a. 312 Ma, Rolland et al., 2013) to its current activity is of about 200 km (Burtman, 1964, 1980). The TFF seems to represent a major discontinuity between east and west Tien Shan as suggested by the distribution of arc magmatism in the MTS: to the west, in the Chatkal Range, a magmatic arc is well-developed whereas to the east the MTS is characterized by a lack of arc magmatism (Fig. 1, Tursungaziev & Petrov, 2008).

2.2. The Chatkal range

The Chatkal Range lies in the MTS to the west of the TFF and to the north of the Fergana basin (Fig. 1). The range is thrusted toward the south upon the Fergana basin along a Cenozoic thrust. The Chatkal Range is mainly made of Upper Paleozoic sediments and metamorphic rocks intruded by Carboniferous arc-related granites and granodiorites (Fig. 2).

During the Silurian, Early and Middle Devonian and during the Pennsylvanian, short-lived arcs evolved in the Chatkal and adjacent areas east of the Talas-Fergana Fault (e.g. Biske, 1996; Seliverstov and Ghes, 2001; Filippova et al., 2001; Alexeiev et al., 2009a; Seltmann et al., 2011) whilst, from the Givetian to the Late

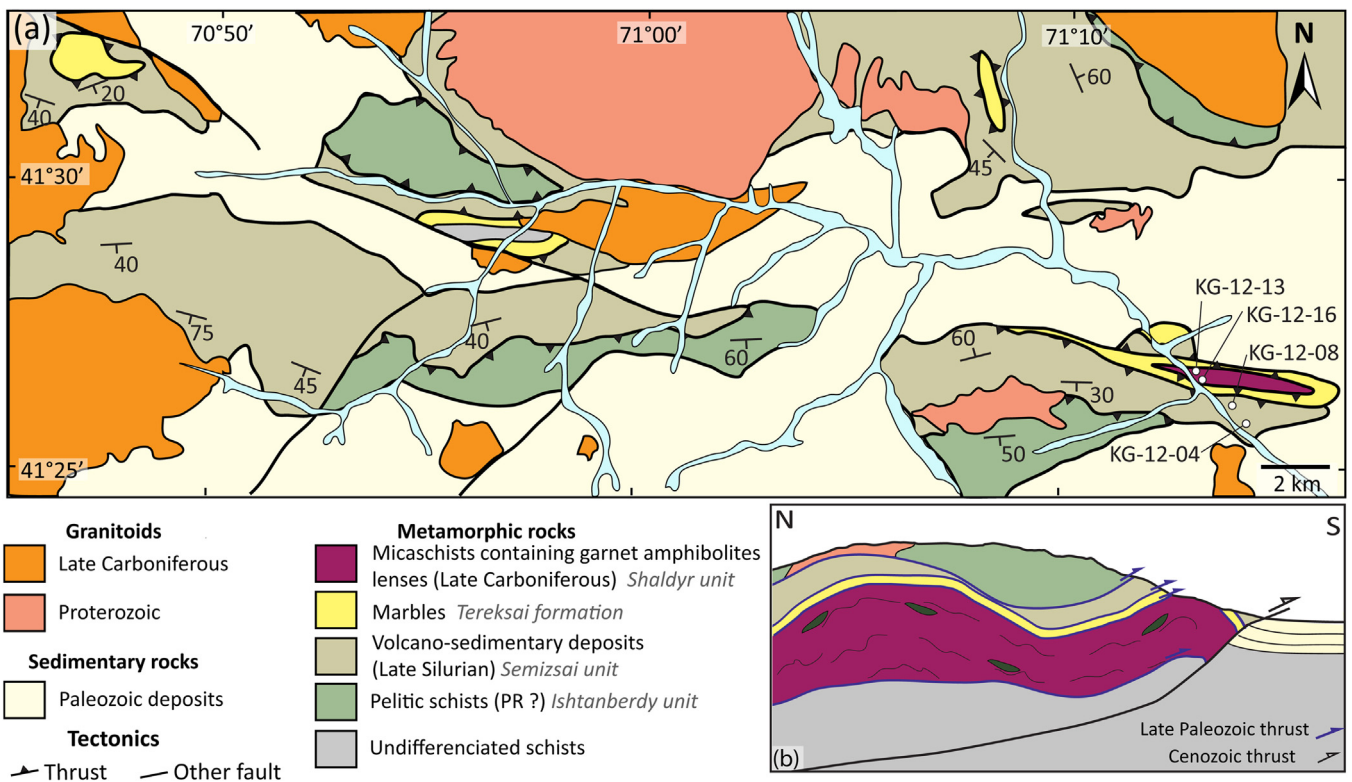


Fig. 2. (a) Geological map of the Chatkal range (modified after Bakirov et al., 2003) and location of samples cited in the text. Location of the map in Fig. 1. Gray italic names are the name of unit after Bakirov et al., 2003. (b) Schematic cross-section of the Chatkal range.

Mississippian, the area represented a passive margin of the Kazakhstan continent (Maksumova et al., 2001; Cook et al., 2002; Alexeiev et al., 2015a,b).

The metamorphic rocks of the Chatkal Range are divided into four units described as follows by Bakirov et al. (2003):

The *Shaldyr unit* is made of schists, gneisses and amphibolites exposed in the core of an anticline. The amphibolites occur as lenses and could contain eclogite facies mineral relics. This unit is thought to be Archean in age (Bakirov et al., 2003) and thus to constitute the continental basement.

The *Tereksei formation* lies upon the Shaldyr unit along a sedimentary unconformity (Turbin, 1962). This formation is made of 600 m thick marbles with rare lenses of quartzite, which were probably deposited in a passive margin setting.

The Tereksei unit is overthrust by the *Semizsai unit*. It is a 4000 m thick unit made of mafic and ultramafic rocks, metapelitic schists and migmatites. Bakirov et al. (2003) interpreted this unit as a metamorphosed ophiolitic sequence reflecting an ancient ocean floor despite the alkaline chemical signature of the metabasites. The migmatites were initially dated at 1920 ± 20 Ma by U-Pb on zircon (Bakirov et al., 1996). However new U-Pb data on detrital zircon grains in a volcanic-derived schist of this unit yield an age of 460.6 ± 1.4 Ma which constrains the maximum age of the protolith to the Middle Ordovician (Rojas-Agramonte et al., 2014). These authors ascribed this volcano-sedimentary unit to volcanic arc activity in this part of the MTS at the end of the Middle Ordovician.

Finally, the Semizsai unit is overlain by the *Ishtanberdy unit*, which is made of low- to medium-grade schists. The base of this unit is made of conglomerates containing pebbles of the underlying Semizsai unit (Bakirov et al., 2003).

As geochronological and petrological data are scarce and controversial, the geodynamic evolution of the Chatkal range remains poorly constrained, especially the tectonic significance of the

presence of the metamorphic rocks. This study aims to provide new structural, geochemical, petrological and geochronological data for the metamorphic rocks of the Chatkal range, especially for the HP relicts of the Shaldyr unit, in order to better understand the geodynamic history of the range.

3. Structure and geochemistry of geological units

3.1. Results of structural and geochemical analysis

Based on previous work (Bakirov et al., 2003), field investigations were carried out and provided new structural data. Representative rocks of each unit were sampled in order to obtain petrological and geochemical data to characterize these units. Fresh samples were crushed and powdered in an agate mill. Bulk-rock analyses were performed at the CRPG of Nancy following the procedure of Carignan et al. (2001). Major-element concentrations were obtained by ICP-OES analyses. The analytical uncertainties are lower than 1% for SiO_2 and Al_2O_3 , 2% for Fe_2O_3 , MgO and CaO , 5% for MnO , K_2O , Na_2O and TiO_2 , and 10% for P_2O_5 . Trace-element concentrations were obtained by ICP-MS analyses. The analytical uncertainties are lower than 5% except for Th, Pb, Zr, Hf and Tm (<10%) and U and Ta (<15%). Results are presented in Table 1 and Fig. 4.

The results lead to revise the geological map and the geodynamic significance of the Chatkal units as follows (Fig. 2):

The *lower unit*, referred as the *Shaldyr unit* by Bakirov et al. (2003), crops out in the core of a WNW-ESE trending anticline (Fig. 3a). It is made of pelitic schists containing quartz, white and black micas, feldspar and millimeter-scale garnet. These schists are strongly foliated in a WNW-ESE direction. Micaschists contain stretched boudins of garnet amphibolites. They contain garnet with amphibole corona and plagioclase, which is typical of

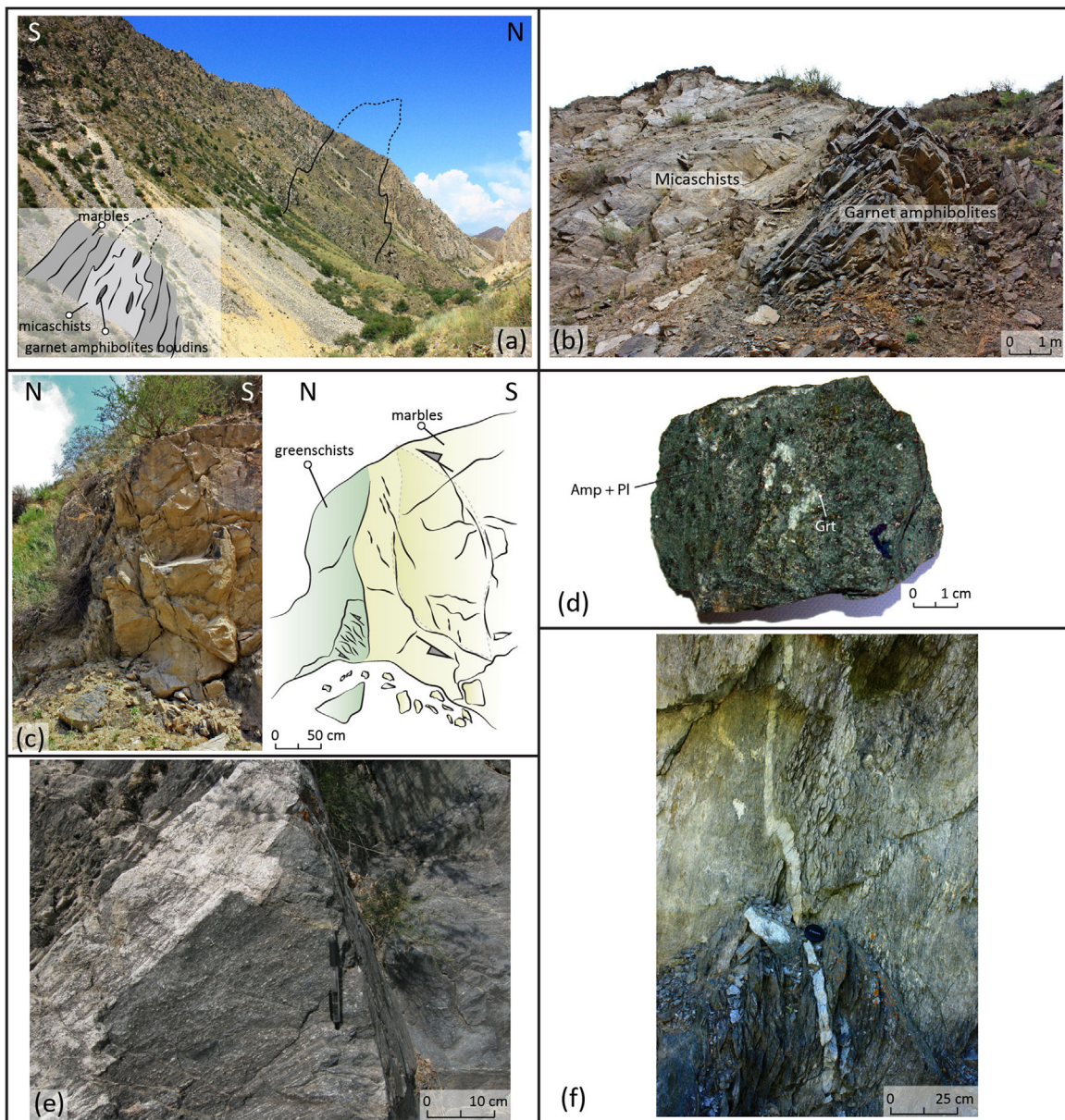


Fig. 3. Field photographs of the studied area. (a) Westward view of an anticline structure with micaschists containing garnet amphibolites lenses in the core. (b) Contact between micaschists (light gray) and a garnet amphibolite lens (dark gray). The lens is pluri-metric in size and is stretched in the lineation strike. (c) Contact between greenschist, in the border of the micaschist/garnet amphibolite unit, and marble showing top north thrusting shearing criteria. (d) Sample of garnet amphibolite (KG-12-16) mainly made of garnet (brownish), and amphibole/diopside/plagioclase symplectite (green, see also Fig. 5d and e). (e) Alternation of amphibolitic (dark) and quartzo-feldspatic (light) layers in the volcano-sedimentary unit indicating a bimodal source volcanism. Evidences of migmatization are seen in the top-left corner. (f) Micaschist containing biotite, muscovite, garnet and staurolite typical of a Barrovian metamorphism. (For interpretation of the references to color in this figure legend, the reader is referred to the web version of this article.)

retrogressed eclogites (Fig. 3b and d). Lenses are about 10 m in width and are several decameters in length. The contact of this unit with the overlying marbles is underlined by a greenschist facies high strain shear zone. Shear criteria at the contact suggest a top-to-the-north sense of shear (Fig. 3c). It indicates that if the initial contact was an unconformity, as suggested by Bakirov et al. (2003), it has been later reactivated as a thrust. The marbles, i.e. the Tereksei formation of Bakirov et al. (2003), are folded in the same WNW-ESE anticline fold as the micaschists. Whole rock geochemical analyses of garnet amphibolites indicate an alkaline composition (Table 1). Total alkali versus silica diagram (Fig. 4a) suggests that the protolith of these metabasites is an alkaline basalt, with 43–48% of SiO₂, 10–18% of Fe₂O₃ and 2–4% of TiO₂. The spider-diagram of garnet amphibolite suggests an OIB-like

composition with very high concentration in Light Rare Earth Elements (LREEs) and lithophile Elements (LILEs), and a relative depletion in Heavy Rare Earth Elements (HREEs) with [(La/Yb)_N = 5.97–6.09] (Fig. 4b).

The volcano-sedimentary unit or Semizsai unit (Bakirov et al., 2003) is made of an alternation of amphibolites, micaschists and leptynites. In some places, the schists are migmatized. This unit does not represent a full ophiolite sequence. In contrast, alternations of feldspar-rich leptynites with more mafic metric layers composed of amphibole and plagioclase could correspond to a volcanic environment with a bimodal source. These volcanic layers alternate with detrital layers of mica-rich metasediments. Such volcano-sedimentary deposits may suggest a volcanic arc setting. In addition, the chemical composition of the amphibolites is in

Table 1

Chemical composition of garnet amphibolites (KG-12-13 and KG-12-16) and amphibolites (KG-12-04 and KG-12-08) from the Chatkal range. La/Yb and Nb/Ce ratios are normalized to primitive mantle compositions (Sun and McDonough, 1989). Samples are located in Fig. 2.

	Garnet amphibolite		Amphibolite	
	KG-12-13	KG-12-16	KG-12-04	KG-12-08
<i>Major elements (ox. wt%)</i>				
SiO ₂	44.57	44.98	57.62	44.49
Al ₂ O ₃	13.21	14.085	17.59	18.178
Fe ₂ O ₃	17.345	9.81	6.913	12.347
MnO	0.29	0.1721	0.1385	0.1722
MgO	6.683	7.274	2.552	7.544
CaO	9.654	12.838	8.416	8.527
Na ₂ O	2.969	3.531	3.38	2.814
K ₂ O	0.219	0.645	0.652	0.983
TiO ₂	3.557	1.891	0.537	1.225
P ₂ O ₅	0.66	0.17	0.18	0.42
PF	-0.03	3.44	1.11	2.02
Total	99.13	98.83	99.08	98.72
<i>Trace elements (ppm)</i>				
Cs	0.16	0.34	0.51	0.77
Rb	5.60	8.73	18.43	32.25
Ba	235.70	134.10	154.10	249.00
Th	1.99	1.53	4.75	0.33
U	0.62	0.47	1.28	0.20
Nb	26.21	15.17	3.37	3.60
Ta	2.09	0.95	0.27	0.25
La	23.99	18.32	14.85	10.60
Ce	52.06	39.48	29.53	24.83
Pb	3.86	3.33	13.55	1.67
Pr	6.50	4.91	3.39	3.52
Sr	203.40	799.80	479.80	563.40
Nd	30.76	22.94	14.42	17.99
Zr	198.50	143.00	93.85	42.21
Hf	4.71	3.58	2.35	1.17
Sm	7.34	5.44	3.06	4.50
Eu	2.55	2.03	0.90	1.38
Gd	7.72	5.60	2.72	4.53
Tb	1.18	0.85	0.40	0.65
Dy	6.77	5.07	2.38	3.74
Y	34.86	28.47	14.07	19.55
Ho	1.27	0.97	0.48	0.71
Er	3.30	2.61	1.39	1.92
Tm	0.44	0.35	0.21	0.26
Yb	2.83	2.20	1.43	1.64
Lu	0.42	0.31	0.23	0.25
La/Yb	6.09	5.97	7.46	4.63
Nb/Ce	1.25	0.96	0.28	0.36

agreement with a volcanic arc setting. Total alkali-silica diagram suggests that the protoliths were basaltic to andesitic in composition ($45\% < \text{SiO}_2 < 58\%$), which is consistent with a calc-alkaline magmatic affinity (Fig. 4a). Spider diagrams show clear negative Nb-Ta anomalies [$(\text{Nb}/\text{Ce})_N = 0.28\text{--}0.36$] associated with strong LILEs and LREEs enrichments [$(\text{La}/\text{Yb})_N = 4.63\text{--}7.46$], which is a typical signature for volcanic arc magmas (e.g. Pearce and Peate, 1995).

The uppermost unit, referred to as the *Ishtanberdy unit* (Bakirov et al., 2003), is made of micaschists containing various proportions of quartz, plagioclase, biotite, muscovite, chlorite, garnet and staurolite. This mineralogy indicates a typical Barrovian type metamorphism linked to a collisional context (e.g., Brown, 1993).

Following these results, the garnet amphibolites lenses wrapped in the micaschists from the HP unit are excellent targets for a detailed petrological and geochronological investigation as they are the unique lithology to preserve both subduction- and collision-related metamorphic imprints.

3.2. Garnet amphibolite description

As described above, the garnet amphibolites crop out as boudins in a micaschist matrix and have a typical texture of retrogressed eclogites. The degree of retrogression varies depending on the samples. The most retrogressed samples contain millimeter-scale plagioclase and green amphibole, garnet with strongly irregular rims, quartz, ilmenite, rutile and local occurrences of clinozoisite. No clinopyroxene was found. Transitional samples contain plagioclase and green amphibole in a first symplectite and clinopyroxene, amphibole and plagioclase associated in a second finer symplectite. Others minerals are garnet, K-feldspar, quartz, rutile, ilmenite and clinozoisite (Fig. 5a–c). The well-preserved samples exhibit fine symplectites of clinopyroxene and plagioclase around garnet, clinozoisite and rutile porphyroblasts. Garnet is surrounded by a thin corona of green amphibole (Fig. 5d and e).

Two samples were chosen for further investigations: in the well-preserved samples, the small size of the symplectite makes it difficult to perform accurate microprobe analysis, especially micro-mapping. Consequently they are not the best suited for petrologic study despite being the best preserved. However, in one of these samples (sample KG-12-16), allanite was found in the core of clinozoisite porphyroblasts (Sample KG-12-16, Fig. 5f). Allanite is a rare earth element rich end-member of the epidote solid solution series: $[\text{Ca},\text{REE},\text{Th}]_2[\text{Fe},\text{Al}]_3\text{Si}_3\text{O}_{12}[\text{OH}]$. It can be dated by in situ U-Pb geochronology and linked to *P-T* conditions based on textural associations with rock-forming minerals in order to obtain *P-T-t* paths (e.g. Janots et al., 2009; Cenki-Tok et al., 2014). In the studied rocks, allanite contains omphacite inclusions suggesting that it is a HP phase. A transitional sample with thicker symplectite was chosen for petrologic and thermobarometric investigations (sample KG-12-13). This kind of sample is well suited to decipher the *P-T* path of the garnet amphibolites as they contain relicts of the HP paragenesis and also minerals of the retrogression stages. Samples are localized on Fig. 2.

4. *P-T* estimates for garnet amphibolites

4.1. Mineral compositions

X-ray maps have been acquired in order to measure the mineral compositions in two dimensions, to constrain the relationships of the different phases and to decipher the *P-T* path of garnet amphibolites. A JEOL JXA-8230 electron probe micro-analyzer at ISTERre laboratory (Grenoble, France) was used to acquire X-ray compositional maps and the spot analyses required for the analytical standardization of the images following the procedure of De Andrade (2006). Analytical conditions for mapping were 15 keV accelerating voltage and 100 nA specimen current. The conditions for spot analyses were 15 keV accelerating voltage and 12 nA specimen current. The maps of 135,000 pixels with 1 μm step size cover an area of 300 μm*450 μm (Fig. 5c). Dwell times were set at 100 ms per pixel. These X-ray maps were processed using the program XMAPTools 1.6.5 (Lanari et al., 2014). Each pixel is assigned to a mineral phase (classification) and then the raw X-ray map is standardized using the spot analyses as internal standards. The intensity maps are converted into maps of weight-percentage composition for each oxide. Then structural formulae maps were calculated on the basis of 12 oxygen for garnet, 6 for clinopyroxene, 23 for amphibole and 8 for feldspar. Fe³⁺ contents were estimated using the method of Holland and Blundy (1994) for amphibole and using the acmite end-member proportion for clinopyroxene and charge-balance. All Fe in garnet is assumed to be Fe²⁺ (as suggested by charge balance computations). Representative analyses of garnet,

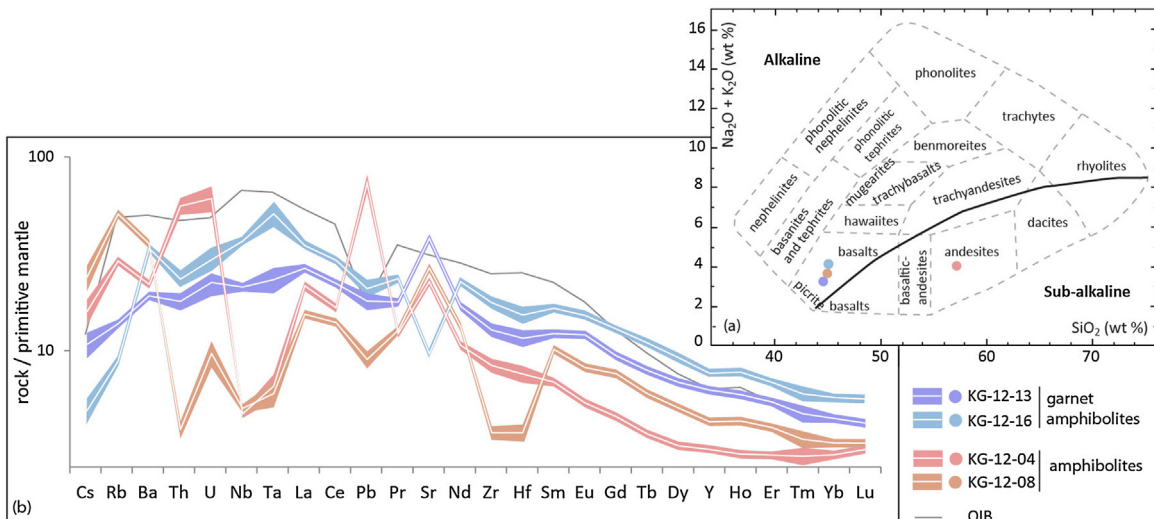


Fig. 4. (a) Total alkali-silica diagram interpreted in terms of protoliths for the garnet amphibolites (open and black circles) and amphibolites (triangles). (b) Spider diagram of studied samples (located on Fig. 2). Open and black circles are for the garnet amphibolites in lenses in micaschists. They have an intraplate composition characterized by enrichment in LREE and depletion in HREE. For comparison, typical OIB composition is shown (Sun and McDonough, 1989). Open and black triangles are for amphibolites from the volcano-sedimentary unit. The depletion in Nb-Ta is typical of subduction context magmas.

clinopyroxene, feldspar and amphibole are reported in Tables 2–5, respectively.

The sample chosen for thermobarometry (KG-12-13) has an intermediate degree of retrogression to properly decipher the sample history from HP to low-P. It is a fine-grained garnet amphibolite mainly made of garnet (20 vol.-%), clinopyroxene-plagioclase-amphibole symplectite (44 vol.-%), amphibole-plagioclase symplectite (34 vol.-%), ilmenite and rutile (~2 vol.-%) (Fig. 5a). Garnet occurs as 0.3–0.5 mm large anhedral grains and contains inclusions of green amphibole, clinozoisite and rutile (Fig. 5b). Garnet has a homogeneous almandine-rich composition (Alm_{66–69}–Grs_{21–23}–Pyr_{08–09}–Sps_{00–01}) (Fig. 6a and b). The rim shows a slightly different composition (Alm₆₅–Grs₂₄–Pyr₀₉–Sps₀₁) but this is more likely due to diffusion along fractures rather than to a growth compositional zoning. Rutile included in garnet suggests that it is a HP phase. No omphacite was found in this rock, thus garnet is the only remaining HP phase. A first fine symplectite (symplectite 1) (lamellae of 10–15 µm) is made of

Table 2

Representative electron microprobe chemical analyses (in oxide wt%) and structural formulae (in pfu) for garnet in KG-12-13 and KG-12-16 samples.

	KG-12-13	KG-12-16
Garnet		
SiO ₂	37.57	38.15
Al ₂ O ₃	21.27	22.10
FeO	29.51	30.61
MnO	0.55	0.35
MgO	2.29	2.37
CaO	8.06	7.98
Na ₂ O	0.01	0.06
K ₂ O	0.04	0.00
Atoms site distribution (12 anhydrous-oxygen basis)		
Si(O/T)	3.01	2.98
Al(Y)	1.99	2.03
Fe(X)	1.98	2.00
Mg(X)	0.26	0.28
Mn(X)	0.00	0.02
Ca(X)	0.69	0.67
XFe	0.68	0.67
XMg	0.09	0.09
XMn	0.00	0.01
XCa	0.24	0.23

Table 3

Representative electron microprobe chemical analyses (in oxide wt%) and structural formulae (in pfu) for clinopyroxene in symplectite in the KG-12-13 sample and for clinopyroxene included in clinozoisite, allanite and garnet in KG-12-16 sample.

KG-12-13	KG-12-16		
	Cpx in symplectite	Cpx included in czo and all	Cpx included in grt
Clinopyroxene			
SiO ₂	52.87	55.59	54.79
Al ₂ O ₃	5.29	9.28	7.37
FeO	8.61	5.58	10.78
MnO	0.11	0.01	0.04
MgO	10.40	8.60	7.36
CaO	17.93	13.90	13.42
Na ₂ O	3.31	6.81	6.78
K ₂ O	0.01	0.00	0.00
Atoms site distribution (6 anhydrous-oxygen basis)			
Si(T1)	1.97	2.00	2.00
Al(T1)	0.03	0.00	0.00
Al(M1)	0.16	0.39	0.32
Mg(M1)	0.61	0.46	0.40
Fe(M1)	0.28	0.15	0.14
Ca(M2)	0.76	0.54	0.53
Na(M2)	0.18	0.48	0.48
XMg	0.68	0.75	0.74

Table 4

Representative electron microprobe chemical analyses (in oxide wt%) and structural formulae (in pfu) for plagioclase in KG-12-13 sample.

	Albite	Orthoclase
Feldspar		
SiO ₂	62.92	58.12
Al ₂ O ₃	17.6	18.04
FeO	1.8	1.93
MnO	0.03	0.02
MgO	0.18	0.1
CaO	2.93	0.44
Na ₂ O	9.98	0.55
K ₂ O	0.04	12.42
Atoms site distribution (8 anhydrous-oxygen basis)		
Si(T)	2.95	2.9
Al(T)	0.98	1.06
Na(M1)	0.97	0.06
Ca(M1)	0.03	0.02
K(M1)	0	0.89

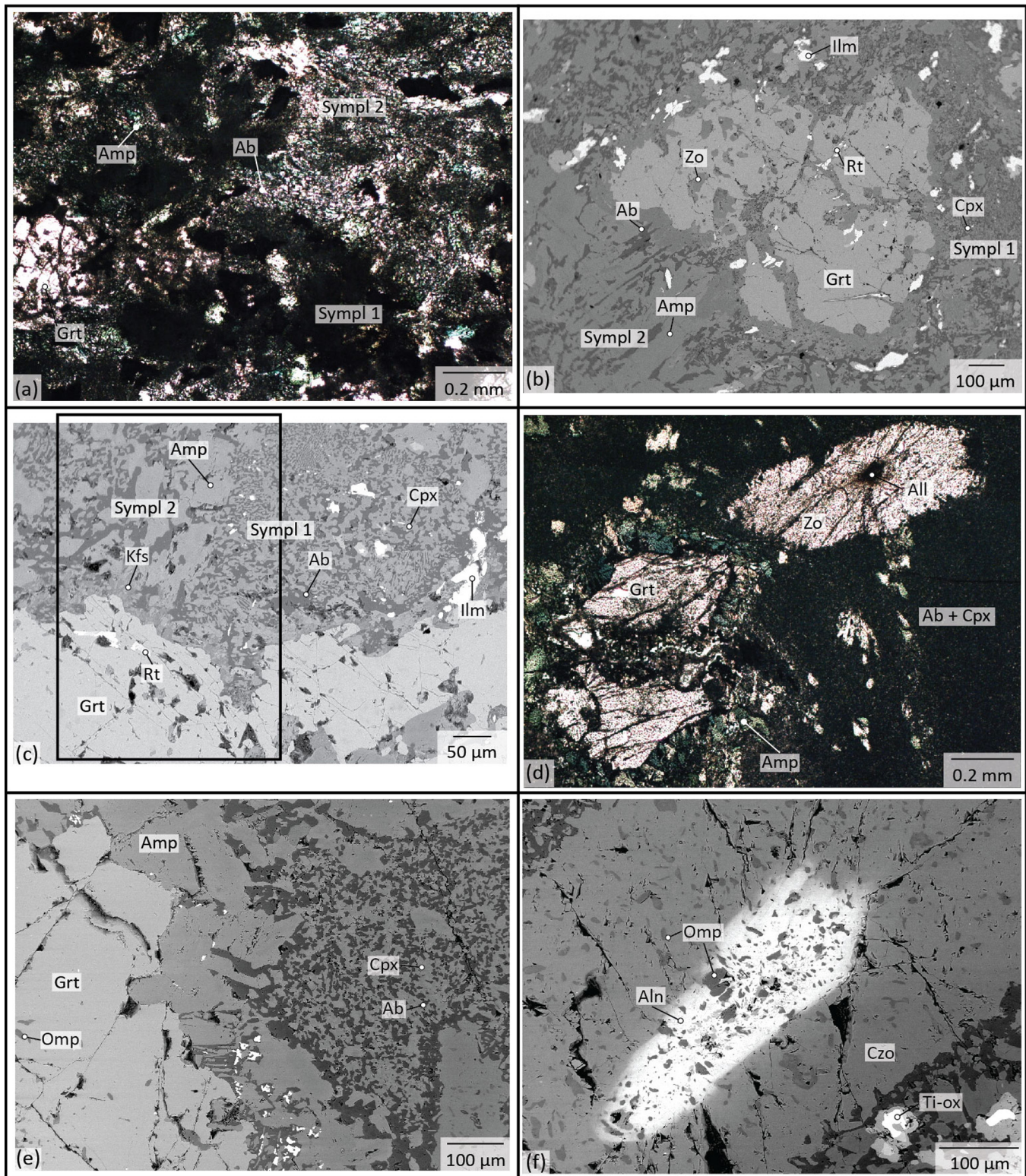


Fig. 5. Photomicrographs of studied retrogressed eclogites (garnet amphibolite) studied samples. (a–c) Sample KG-12-13: intermediate degree of retrogression. (a) Garnet and symplectites in plane polarized light. Garnet is strongly retrogressed, with irregular rims. Two types of symplectites can be distinguished: amphibole and albite (small green and white grains, Sympl. 1), and diopside, albite and amphibole (dark areas, Sympl. 2). (b) Back-scattered-electron (BSE) image of a garnet with clinzozoisite, amphibole and rutile inclusions. The two types of symplectites (Sympl. 1 and 2) are visible around the garnet. (c) BSE image of the selected area for micro-mapping (black frame) with garnet and the two types of symplectites. (d–f) Sample KG-12-16: less retrogressed sample. (d) Microphotography in plane polarized light. The dark green matrix is constituted by a very fine-grained symplectite of clinopyroxene and albite. Garnet and clinzozoisite occur as porphyroblasts. Garnet is surrounded by a green amphibole corona. Allanite is found in the core of clinzozoisite (dark brown). (e) BSE image of a garnet, its surrounding green amphibole corona and the clinopyroxene-albite symplectite. Omphacite with high jadeite content is included in garnet. (f) BSE image of an allanite (highly reflective) in the core of a clinzozoisite. Both the allanite and the clinzozoisite contain omphacite inclusions with high jadeite contents (Jd_{36}) suggesting that they are HP phases. (For interpretation of the references to color in this figure legend, the reader is referred to the web version of this article.)

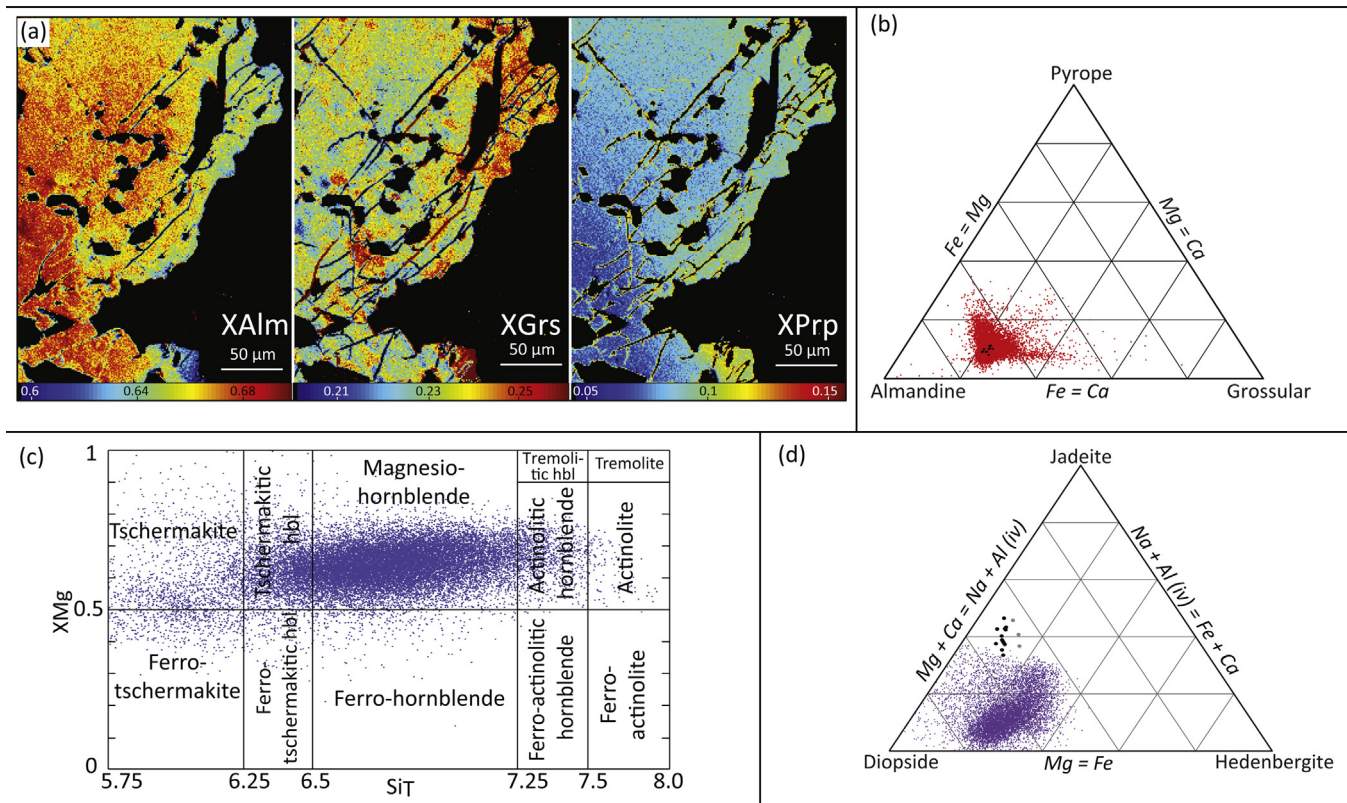


Fig. 6. Mineral compositions of garnet amphibolite (see Section 5.2 for data for KG-12-16 sample). See Tables 2–5 for representative analysis of garnet, clinopyroxene, albite and amphibole, respectively. (a) Map of almandine, grossular and pyrope content of garnet of the KG-12-13 sample. The composition is rather homogeneous with a slightly different rim probably due to diffusion. (b) Triangular diagram almandine-pyrope-hedenbergite showing the composition of garnet of the KG-12-13 (red points) and KG-12-16 samples (black points). (c) Composition of amphibole of the KG-12-13 sample following the classification of Leake (1978). (d) Triangular diagram diopside-jadeite-hedenbergite showing the composition of clinopyroxene in the first symplectite of the KG-12-13 sample (purple points) and of clinopyroxene included in epidote and allanite (black points) and garnet (gray points) of the KG-12-16 sample. (For interpretation of the references to color in this figure legend, the reader is referred to the web version of this article.)

clinopyroxene, amphibole and plagioclase (Fig. 5c). Clinopyroxene has a diopside composition ($\text{Di}_{61-70}\text{-Jd}_{7-18}\text{-Hd}_{22-30}$) with jadeite content decreasing from the core toward the rim (Jd_{18-7}) (Fig. 6c). Plagioclase has a homogeneous and nearly pure albitic composition (Ab_{94-98}). Amphibole is pale green and has a magnesio-hornblende

composition following the classification of Leake (1978). Minor Ti-oxides occur in this symplectite such as rutile or ilmenite. A second symplectite (symplectite 2), wider than the first one (lamellae of 20–40 μm), is made of amphibole and plagioclase (Fig. 5c) without any clinopyroxene. Amphibole has a similar magnesio-hornblende composition as the one of symplectite 1 and plagioclase has also a nearly pure albitic composition (Ab_{94-98}). Amphibole nearby garnet has a different chemical composition with higher Al (~3.0 pfu) and Fe (~2.5 pfu) contents indicating a chemical interaction with the garnet (Fig. 7a and b). Consequently, for the following thermobarometric calculations implying amphibole, only the compositions of amphibole “away” from the garnet were taken into account as those close to the garnet may have been strongly affected by the interactions with it. Based on the textural relationships, the two different symplectites may thus represent two stages of retrogression. Symplectite 1, with preserved clinopyroxene, was probably formed during early stages of exhumation while symplectite 2, without clinopyroxene, may have formed at a later stage. Thus, the garnet and the two symplectites represent three different assemblages corresponding to distinct stages along the P - T path. The compositional maps also highlighted a K-feldspar corona around the garnet (Fig. 5c). Although K-Feldspar is rare in mafic lithologies, it might have crystallized here because of a local excess of potassium due to the alkaline composition of that rock.

Table 5
Representative electron microprobe chemical analyses (in oxide wt%) and structural formulae (in pfu) for amphibole in KG-12-13 sample.

Amphibole	
SiO_2	44.23
Al_2O_3	10.65
FeO	16.75
MnO	0.14
MgO	10.33
CaO	10.17
Na_2O	2.29
K_2O	0.25
Atoms site distribution (23 anhydrous-oxygen basis)	
$\text{Si}(\text{T1})$	4
$\text{Si}(\text{T2})$	2.92
$\text{Al}(\text{T2})$	1.06
$\text{Al}(\text{M2})$	0.45
$\text{Mg}(\text{M2})$	0.85
$\text{Fe}(\text{M2})$	0.68
$\text{Mg}(\text{M13})$	1.74
$\text{Fe}(\text{M13})$	1.38
$\text{Ca}(\text{M4})$	1.82
$\text{Na}(\text{M4})$	0.18
$\text{Na}(\text{A})$	0.4
$\text{Vac}(\text{A})$	0.6
XMg	0.55
XFe	0.44

4.2. Thermobarometry

In order to reconstruct the P - T path of the garnet amphibolite, rock-specific equilibrium phase diagrams (elsewhere called

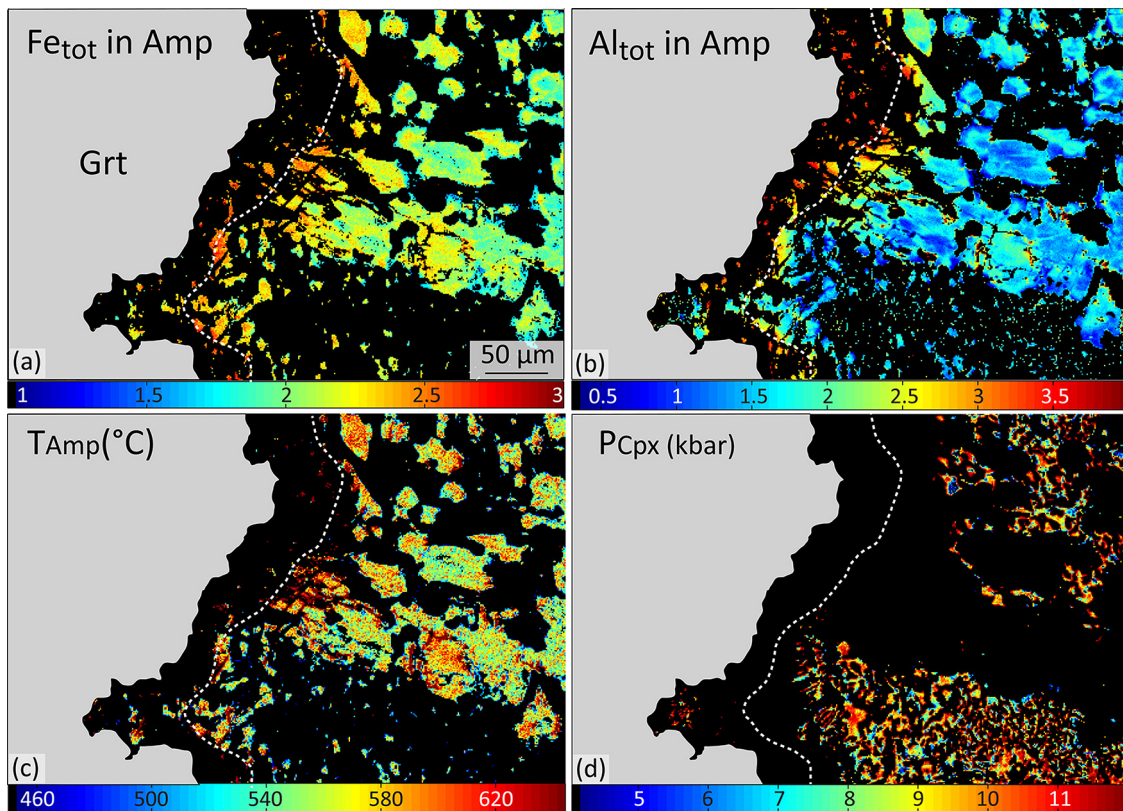


Fig. 7. Compositional maps of amphibole compared with temperature and pressure maps. Gray area represents the present garnet. White dashed line represents the supposed initial border of garnet. Map of total iron (a) and aluminum (b) contents in amphibole. Fe and Al contents strongly increase toward the garnet (shaded gray area) suggesting a chemical interaction between garnet and amphibole. (c) Temperature map for amphibole obtained with the calibration of Holland and Blundy (1994) with fixed composition of plagioclase. The temperature estimates in the area of chemical interaction between garnet and amphibole seem to be higher and are thus considered as no relevant. (d) Pressure map for clinopyroxene obtained with the calibration of Waters (2002, 2003) with fixed composition of amphibole and plagioclase.

pseudosection) and empirical and semi-empirical calculations were used. The P - T equilibrium phase diagram was calculated with the Theriault-Domino software (De Capitani & Petrakakis, 2010) using the internally consistent thermodynamic data set of Berman (1988) and subsequent updates (JUN92.bs). The chemical system considered was NCFMASHTO (Na_2O , CaO , FeO , MgO , Al_2O_3 , SiO_2 , TiO_2 , H_2O , O). As K-feldspar is the only K-rich phase and only occurs as the result of ultra-local equilibria, the system was simplified by excluding K_2O . The same simplification was done for MnO , which has negligible amount in all measured phases. The solid solution models used were those of Berman (1988) in JUN92.bs except for omphacite (Meyre et al., 1997), chlorite (Hunziker, 2003) and white micas (Keller et al., 2005).

In a first step, the effective bulk composition used for phase diagram calculation was supposed to be the bulk-rock composition measured by ICP-OES. However, the model did not match the observations, especially concerning the garnet compositions. Therefore we used another composition based on mineral abundance and their composition of each local assemblages (Warren & Waters, 2006; Lanari et al., 2013). The modal abundance of garnet (~20%), fine symplectite (~45%) and wide symplectite (~35%) were calculated by a thin-section optical image analysis and their composition was calculated from the standardized X-ray map using the function local effective bulk available in XMPTOOLS. The obtained local effective bulk composition was used for phase diagram calculation over a pressure range of 1–25 kbar and a temperature range of 350–600 °C.

The equilibrium phase diagram is shown on Fig. 8. For the metamorphic peak conditions, garnet composition isopleths were calculated to determine the P - T conditions of

their crystallization. The garnet composition observed on the map ($\text{Alm}_{66-69}-\text{Grs}_{21-23}-\text{Pyr}_{08-09}$) is best modeled at 490 °C and 18.5 kbar ($\text{Alm}_{71}-\text{Grs}_{21}-\text{Pyr}_{08}$). The corresponding stable assemblage at these conditions is garnet, omphacite, chlorite, rutile, quartz, paragonite and H_2O . However, only rutile was preserved as inclusions in garnet.

During a first stage of retrogression, omphacite was retrogressed into diopside, amphibole and plagioclase forming symplectite 1. The temperature conditions for the crystallization of this symplectite were estimated using the calibration of Holland and Blundy (1994) based on the distribution of Na and Ca between plagioclase and amphibole. Calculations were performed for each amphibole pixel with a fixed plagioclase composition determined from the map ($\text{Ab}_{97}-\text{An}_{03}$). The obtained temperature is 560 ± 40 °C (Fig. 7c). The higher temperatures (>620 °C) obtained at the garnet rim are explained by the compositional variability in amphibole caused by its chemical diffusion exchange with garnet. The pressure was then estimated for the average temperature of 560 °C using the calibration of Waters (2002, 2003) based on the reaction jadeite + tremolite = albite + edenite. Activities of involved end members were calculated following the models of Dale et al. (2000) for amphibole and Holland (1990) for clinopyroxene and were considered as ideal for plagioclase. Calculations were performed for each clinopyroxene pixel with a fixed plagioclase and amphibole compositions determined from the map (details in Lanari et al., 2013). Pressure estimates range from 11 to 8 kbar from clinopyroxene core to rim (Fig. 7d). In complement, the isopleths of jadeite content in clinopyroxene were modeled in the P - T section (Fig. 8). The jadeite content of clinopyroxene varies from 0.19 to 0.09 at 11 and 8 kbar, respectively. This result is in line with observations

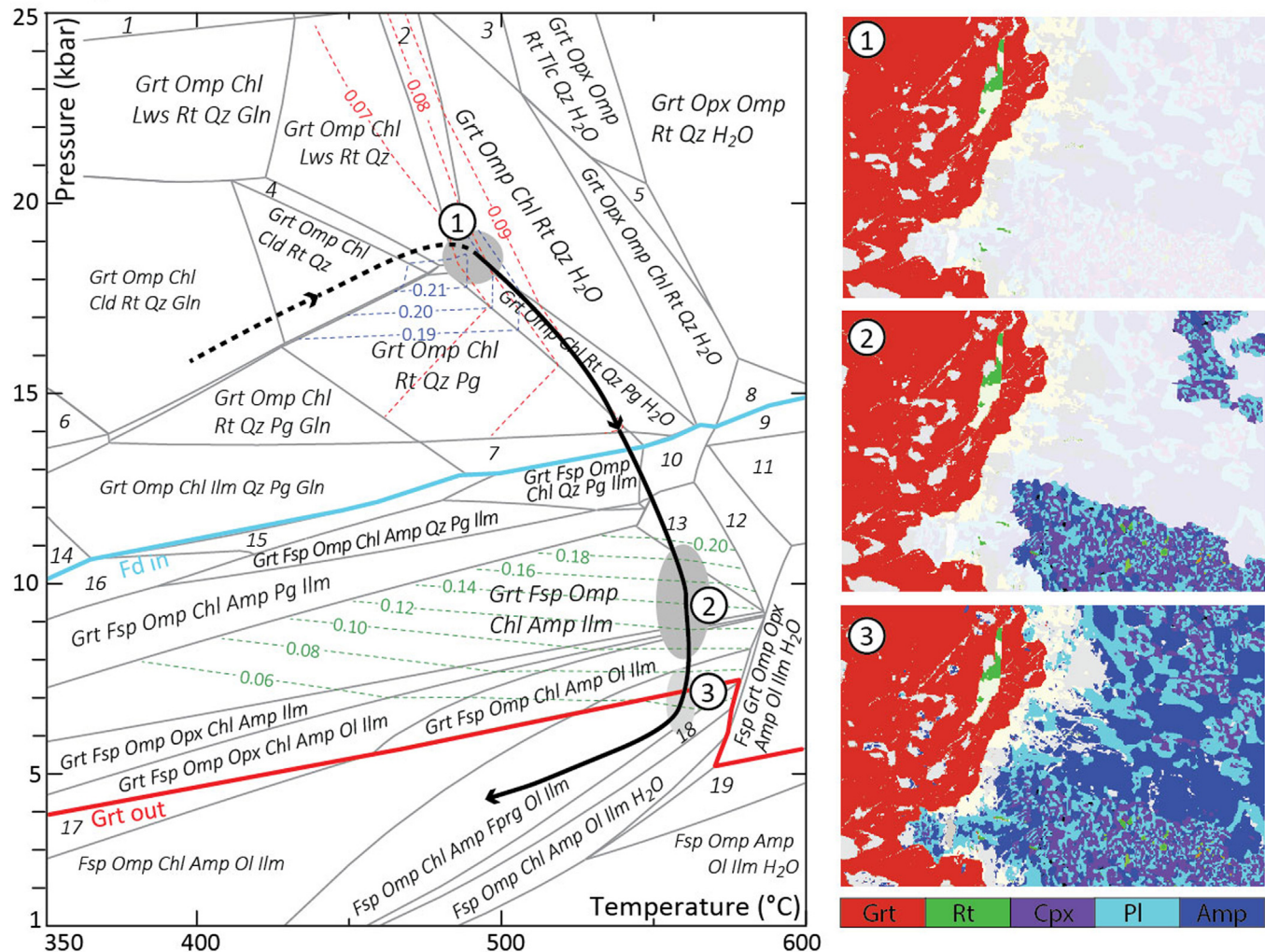


Fig. 8. Pseudosection calculated in the NCFMASHTO system using the Theriault-Domino software (De Capitani & Petrakakis, 2010) from the effective composition: Si(0.823) Al(0.249) Fe(0.192) Mg(0.172) Ca(0.181) Na(0.130) Ti(0.007) H(0.25) O(?). The numbered gray areas represent *P-T* estimates for the three paragenesis represented on the right (only the phases used for *P-T* estimations are shown): 1-garnet, 2-clinopyroxene-amphibole-plagioclase symplectite, 3-amphibole-plagioclase symplectite (*P* conditions are not constrained directly). The obtained *P-T* path is drawn in bold black line. Pyrope and grossular content in garnet and jadeite content in clinopyroxene isopleths are represented in red, blue and green dashed lines, respectively. Feldspar-in and garnet-out reactions are shown in light blue and red solid lines, respectively. Numbered fields: 1-Grt Omp Chl Lws Rt Coe Gln, 2-Grt Omp Chl Lws Rt Qz H₂O, 3-Grt Opx Rt Tlc Qz H₂O, 4-Grt Omp Cld Lws Rt Qz, 5-Grt Opx Omp Gln Rt Qz H₂O, 6-Omp Chl Cld Ilm Rt Gln, 7-Grt Omp Chl Qz Pg Ilm, 8-Grt Opx Amp Omp Rt Qz H₂O, 9-Grt Fsp Opx Amp Omp Rt Qz H₂O, 10-Grt Fsp Omp Chl Qz Ilm H₂O, 11-Fsp Grt Omp Opx Chl Amp Ilm H₂O, 12-Fsp Grt Opx Amp Ilm H₂O, 13-Fsp Grt Omp Amp Ilm H₂O, 14-Grt Omp Chl Ilm Pg Gln, 15-Grt Fsp Omp Chl Ilm Qz Pg Gln, 16-Grt Fsp Omp Chl Ilm Pg Gln, 17-Fsp Opx Chl Amp Ol Ilm, 18-Fsp Omp Chl Amp Fprg Ol Ilm H₂O, 19-Fsp Opx Amp Ol Ilm H₂O. Abbreviations used are after Whitney and Evans (2010): Amp-amphibole, Chl-chlorite, Cld-chloritoid, Coe-coesite, Fprg-ferry-pargasite, Fsp-feldspar, Gln-glaucophane, Grt-garnet, Ilm-ilmenite, Lws-lawsonite, Ol-olivine, Omp-omphacite, Opx-orthopyroxene, Pg-paragonite, Qz-quartz, Rt-rutile. (For interpretation of the references to color in this figure legend, the reader is referred to the web version of this article.)

(Jd_{18→7} from core to rim) and with the pressure estimates from the calibration of Waters (2002, 2003).

Symplectite 2 was formed during a second stage of retrogression. The absence of clinopyroxene in this symplectite prevents the estimation of pressure using the calibration of Waters (2002, 2003). However the temperature can also be estimated with the calibration of Holland and Blundy (1994). Similar to symplectite 1, calculations were performed for each amphibole pixel with a fixed plagioclase composition (Ab₉₇-An₀₃). The estimated temperatures of 560 ± 30 °C, are similar to those obtained for amphibole of symplectite 1. The pressure cannot be directly estimated. However, the rim of amphibole 2 (Fe_{tot} = 2.3, Al_{tot} = 1.8) is slightly enriched in Fe and Al compared to its core (Fe_{tot} = 1.9, Al_{tot} = 1.2, Fig. 7a and b). This suggests that the rim of amphibole 2 crystallized during garnet breakdown, precisely when more Al and Fe are available, which corresponds to pressure lower than 7 kbar according to the *P-T* section (Fig. 8).

5. Allanite dating

5.1. Methods

Allanite is a rare earth element (REE) rich end-member of the epidote solid solution series ([Ca,REE,Th]₂[Fe,Al]₃Si₃O₁₂[OH]). The mineral is key to the storage and mobility of REE, Th and U (Hermann, 2002; Giere and Sorensen, 2004), and offers geochronological information that can be linked with physico-chemical conditions (e.g., pressure, temperature conditions), based upon petrological observations.

LA-ICPMS U-Pb dating of allanite was performed in situ on ca. 100 µm thick thin sections. Allanite was analyzed at the University of Montpellier 2 (Géosciences Montpellier, AETE regional facility) using a Thermo-Finnigan Element XR sector field ICPMS (ThermoFisher Scientific, Germany and USA) coupled to a GeoLas Q+ CompEx-102 193 nm ArF excimer laser ablation system (Lambda

Table 6

LA-ICPMS allanite isotopic data for garnet amphibolite sample KG-12-16 and for reference material BONA.

Identifier	Raster (μm)	$\text{U}^{238}/\text{Pb}^{206}$	1σ perc	$\text{Pb}^{207}/\text{Pb}^{206}$	1σ perc
ALLANITE KG12-16					
hc.1	26*40	5.933	0.665	0.622	1.068
hc.2	26*40	5.436	0.669	0.645	1.067
hc.3	26*40	5.536	0.670	0.643	1.069
hc.4	26*40	4.652	0.693	0.675	1.084
hc.5	26*40	4.869	0.677	0.660	1.072
hc.6	26*40	3.876	0.674	0.695	1.065
hc.7	26*40	4.537	0.685	0.679	1.075
hc.8	26*40	3.682	0.685	0.720	1.071
hc.9	26*40	4.092	0.692	0.702	1.075
hc.10	26*40	5.244	0.687	0.646	1.074
hc.11	26*40	4.020	0.687	0.703	1.070
hc.12	26*40	4.319	0.713	0.707	1.086
hc.13	26*40	5.403	0.686	0.640	1.070
hc.14	26*40	5.195	0.691	0.665	1.071
hc.15	26*40	3.986	0.702	0.703	1.075
na.1	26*40	5.529	0.818	0.671	1.048
na.2	26*40	5.979	0.813	0.648	1.045
na.3	26*40	2.478	0.895	0.786	1.099
na.4	26*40	5.801	0.806	0.664	1.041
na.5	26*40	6.085	0.797	0.636	1.036
na.6	26*40	4.769	0.806	0.705	1.046
na.7	26*40	5.183	0.793	0.672	1.037
na.8	26*40	4.753	0.794	0.683	1.037
na.9	26*40	0.411	1.443	0.851	1.285
na.10	26*40	0.326	2.143	0.830	1.717
na.11	26*40	3.947	0.793	0.701	1.040
na.12	26*40	0.366	1.130	0.864	1.109
na.13	26*40	2.316	0.806	0.772	1.043
na.14	26*40	4.668	0.784	0.688	1.036
na.15	26*40	0.327	1.852	0.846	1.351
na.16	26*40	0.422	0.976	0.847	1.071
na.17	26*40	0.100	3.526	0.853	1.556
na.18	26*40	0.230	1.500	0.869	1.165

Physik, Germany). Analytical protocols and instrument conditions followed those described in detail by Darling et al. (2012). Key points of the methodology are: (a) 40- μm long line-raster ablation, in order to minimize time-dependent elemental fractionation; (b) external normalization of the $^{206}\text{Pb}/^{238}\text{U}$ ratios using the zircon standard 91500 (Wiedenbeck et al., 2004). The laser was generally operated at a repetition rate of 6 Hz, beam diameter of 26 μm with a density of c. 10 J/cm². Each analysis was preceded by a pre-ablation of the surface using a beam diameter of 77 μm . He was used as a cell gas. The ThO^+/Th^+ ratio was optimized to be <1.0%. The acquisition times for the background and the ablation interval amounted to about 15 and 45 s, respectively. Data were reduced using the Glitter program (Jackson et al., 2004). Intervals of 30 s were selected in the signal and checked before the integration of time-resolved signals to avoid possible contamination by mineral inclusions. As allanite is generally enriched in common Pb, Tera-Wasserburg diagrams (Tera and Wasserburg, 1972) were employed and generated by Isoplot version 3.41 (Ludwig, 2003). Because we used a non-matrix-matching standard for allanite, accuracy of the results was monitored by several analyses of a secondary reference material BONA (Gregory et al., 2007). During the course of this study, analyses of the BONA reference material yielded a Tera-Wasserburg regression age of 39.9 ± 5.3 Ma (MSWD = 3.5), which is within uncertainties of reference values (see Darling et al., 2012). Common lead uncorrected $^{238}\text{U}/^{206}\text{Pb}$ and $^{207}\text{Pb}/^{206}\text{Pb}$ ratios obtained for the BONA allanite standard during the past 2 years are $31.056 \pm 1.074\%$ and $0.691 \pm 1.318\%$ ($n=32$), respectively (Table 6).

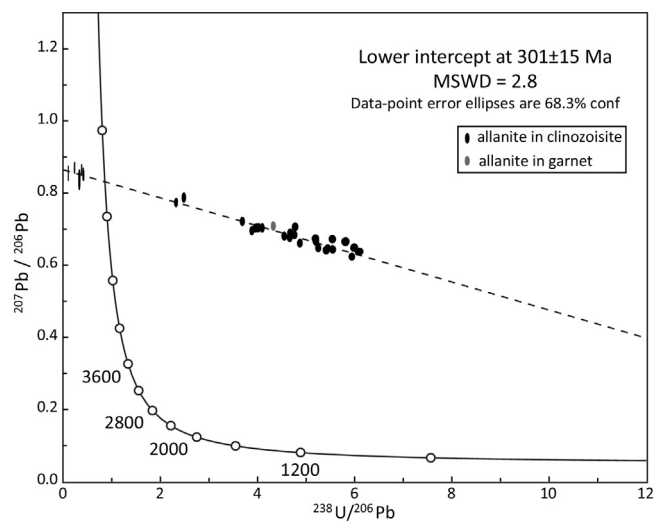


Fig. 9. Tera-Wasserburg diagram for allanite grains (sample KG-12-16) dated in situ on thick sections by LA-ICPMS.

5.2. Age of the HP stage

The sample chosen for U-Pb geochronology (KG-12-16) is a very fine-grained garnet amphibolite composed of a matrix made of clinopyroxene-albite symplectite as well as garnet, clinozoisite and Ti-oxides porphyroblasts. The clinopyroxene and albite symplectite is very fine grained (5–10 μm). Clinopyroxene has a diopside composition (Di₇₉-Jd₀₈-Hd₁₁). In this matrix garnet and clinozoisite occur as porphyroblasts. Garnet is 0.5–2 mm in width and has an almandine composition (Alm₆₇-Grs₂₃-Pyr₀₉, Fig. 6b, Table 2). It contains inclusions of green amphibole and omphacite with a jadeite content ranging from 32 to 40% (Fig. 6d, Table 3). Garnet is surrounded by a green amphibole corona of 0.1–0.3 mm in width. Clinozoisite occurs as porphyroblasts 1–2 mm in length and 0.5–1 mm in width. Allanite occurs in the core of clinozoisite crystals and sometimes as inclusions in garnet (Fig. 5d and f). These are brownish crystals, 50–80 μm long and 30–60 μm wide. Allanites included in garnet are generally too small to be dated, thus only one such allanites was analyzed. Both clinozoisite and allanite contain omphacite inclusions with jadeite contents ranging from 30 to 40%.

Empirical thermobarometry was performed on this sample in order to link geochronological data with the more detailed P-T estimates obtained from the other sample. The garnet-clinopyroxene thermometer of Ravna (2000) yields temperature ranging from 440 to 524 °C. A minimum pressure can be estimated from the reaction albite = jadeite + quartz (Holland, 1983). In the absence of prograde albite, the maximum jadeite content of omphacite included in allanite and garnet of 40% indicates minimum pressure of 11 and 12 kbar at 440 and 525 °C respectively. These P-T estimates are consistent within errors with previous P-T estimates for the sample KG-12-13 (490 ± 50 °C and 18.5 ± 2 kbar). These results suggest that the allanite crystallized during the high-pressure stage.

In situ U-Pb dating of these allanite grains yield a lower intercept Tera-Wasserburg age of 301 ± 15 Ma (MSWD = 2.8; $n=33$; Fig. 9; Table 6). The data points are scattered along a discordant line in the Tera-Wasserburg diagram because the allanite grains could have incorporated variable amounts of common Pb upon crystallization or variable amounts of U leading to variable amounts of radiogenic Pb and thus variable fractions of common Pb. The only analysis of allanite included in garnet is on the same line as the allanites included in clinozoisites (Fig. 9). Moreover, as the MSWD is lower than 3, from a statistical point of view we can assume that the

analyses can all be modeled with two end-members. Consequently it suggests that the allanite have crystallized at the same time and from a well homogenized common lead composition at the sample scale.

The regression of the analyses in a Tera–Wasserburg diagram yields an initial $^{207}\text{Pb}/^{206}\text{Pb}$ ratio of 0.8646. This result is in accordance with the ratio predicted by Stacey & Kramers (1975) at 300 Ma indicating that the allanite crystallized from a Pb composition close to the Earth Pb evolution model. It strengthens the hypothesis that data scattering is due to incorporation of variable amounts of common Pb upon crystallization rather than opening of the system during retrogression. The omphacite inclusions with high jadeite contents in allanite and the results of empirical thermobarometry suggest that allanite growth is related to the HP stage. We therefore consider this Tera–Wasserburg lower intercept U–Pb age obtained for allanite as the age for the HP stage.

6. Discussion

6.1. Deciphering the P–T–t path of retrogressed eclogites

Deciphering the P – T – t path of HP rocks brings important information about vertical motions in the lithosphere during subduction and collision processes (e.g., Duchene et al., 1997). However, when these rocks subsequently suffer a collisional event, the HP metamorphism can be strongly overprinted by amphibolite or granulite facies metamorphism (e.g., Mercier et al., 1991; Lanari et al., 2013). In this case it remains difficult to determine both (i) the P – T conditions that affected the rock before its retrogression and (ii) the age of the HP stage. The micro-mapping approach (Lanari et al., 2012, 2014) combined with in situ dating of preserved HP phases (e.g., Rubatto and Hermann, 2001) is well adapted to solve these problems.

6.1.1. P–T path obtained from micro-mapping

In this study, micro-mapping of garnet amphibolites highlights textural relationships between different parageneses and allows to constrain the P – T conditions of the HP stage and of the subsequent retrogression stages (see Section 4.2). The metamorphic peak conditions are estimated at $490 \pm 50^\circ\text{C}$ and 18.5 ± 2 kbar, which corresponds to the lower temperature boundary of eclogite facies following Evans (1990). The HP paragenesis was characterized mainly by garnet and omphacite (\pm chlorite, rutile, quartz), which is a typical eclogite facies assemblage. During exhumation, the eclogite was retrogressed into garnet amphibolite. Two successive stages of retrogression were preserved in the rock. A first stage, marked by the breakdown of omphacite into diopside, amphibole and Na-plagioclase, occurred between 11 and 8 kbar at $560 \pm 50^\circ\text{C}$. A second stage, marked by the crystallization of amphibole and plagioclase without clinopyroxene, occurred at lower pressures and probably ended at pressure less than 7 kbar at a similar temperature of $560 \pm 50^\circ\text{C}$. The P – T path obtained from these P – T estimates (Figs. 8 and 11) implies a burial along a cold geothermal gradient of $\sim 8^\circ\text{C/km}$, assuming lithostatic pressure, which is typical for subduction zones (e.g., Peacock, 1996). During the exhumation following the pressure peak until the first retrogression stage, the temperature increased from 490 to 560°C , and remained at 560°C until at least 7 kbar implying a geothermal gradient of $\sim 24^\circ\text{C/km}$ at the second retrogression stage assuming lithostatic pressure. This increase of geothermal gradient from 8 to 24°C/km between the subduction and exhumation stages suggests that the HP rocks were probably exhumed when a significant change in geodynamic setting occurred, such as the transition from subduction to collision (see Section 6.3).

6.1.2. Dating HP metamorphism with allanite

In the case of preserved eclogites, the HP stage can be dated by different systems implying garnet or phengite such as Sm–Nd, Lu–Hf, Rb–Sr or Ar–Ar or by in situ geochronology such as U–Pb in zircon (e.g. Hacker and Wang, 1995; Duchene et al., 1997; Rubatto et al., 1999; De Sigoyer et al., 2000). When the subduction-related metamorphic assemblages are partially overprinted, garnet and other HP phases are generally retrogressed and cannot be used for geochronology (e.g. Schneider et al., 2008). The in situ dating of preserved HP phases is thus the only way to date the HP stage, even if it remains difficult due to generally zoned minerals (e.g. Riel et al., 2008). Allanite is a useful and robust chronometer to date HP metamorphism in eclogites and felsic gneisses (De Sigoyer et al., 2000; Parrish et al., 2006; Smey et al., 2011; Regis et al., 2014), as well as to date prograde Barrovian metamorphism in metapelites (Janots et al., 2009; Janots and Rubatto, 2014) or mylonites formed under greenschist facies conditions (Cenki-Tok et al., 2014). In this study, we used allanite texturally associated with omphacite in order to date HP metamorphism in retrogressed mafic eclogites. Located in the core of clinozoisite, or more rarely in garnet, allanite has been preserved from retrogression. Chemical and mechanical shielding of allanite allowing for the preservation of the age record of early metamorphic events has already been reported (Cenki-Tok et al., 2011). Our results show the potential of allanite to date HP events even when subduction-related metamorphism has been overprinted by a significant high temperature event. In this case, allanite has been enclosed in the core of clinozoisite and was thus preserved from reaction with apatite to form monazite.

The P – T and time constraints were acquired on two different samples. However these samples came from the same geological unit. Moreover, the two samples underwent the same P – T condition as suggested by empirical thermobarometry on the sample used for geochronology. This suggests that even if P – T and time constraints were obtained on two different samples, the results can be combined to reconstruct a P – T – t path (Fig. 11).

This study brings key information for the geodynamic history of the area. In the case of the Chatkal range, this is the first report of HP metamorphism. The obtained age of 301 ± 15 Ma is a Tera–Wasserburg lower intercept age and other datings with different isotopic systems could strengthen this age for the HP stage. Moreover the obtained P – T – t path considerably improves the understanding of the area. Our data show that the HP metamorphism is significantly younger than previously suggested (Bakirov et al., 2003) and that it can be correlated with the Late Carboniferous accretion of the Tarim Craton, which is well established to the east of TFF (Hegner et al., 2010), as discussed below.

6.2. Geodynamic evolution of the Chatkal range

The obtained petrological and geochronological data provide further information in order to constrain the Chatkal range history in the Late Paleozoic times. Combined with previously published data, they allow to propose a new geodynamic evolution model for the Middle and South Tien Shan blocks, to the west of the TFF (Fig. 10).

The northward subduction of the Turkestan Ocean under the southern margin of Kazakh Platform probably began in the Late Silurian-Early Devonian (Fig. 10a, Biske, 1996; Seliverstov and Ghes, 2001; Filippova et al., 2001; Alekseev et al., 2009b; Seltmann et al., 2011) leading to the formation of a continental volcanic arc in the Middle Tien Shan. The volcano-sedimentary unit observed in the Chatkal range is dated at 460 Ma (Rojas-Agramonte et al., 2014). It is therefore not linked to the Turkestan Ocean closure. Rather, it might have formed in a previous volcanic arc, when the Middle Tien Shan was still attached to the North-Tarim or North-East Gondwana margin (e.g. Von Raumer et al., 2002, 2003; Von Raumer and

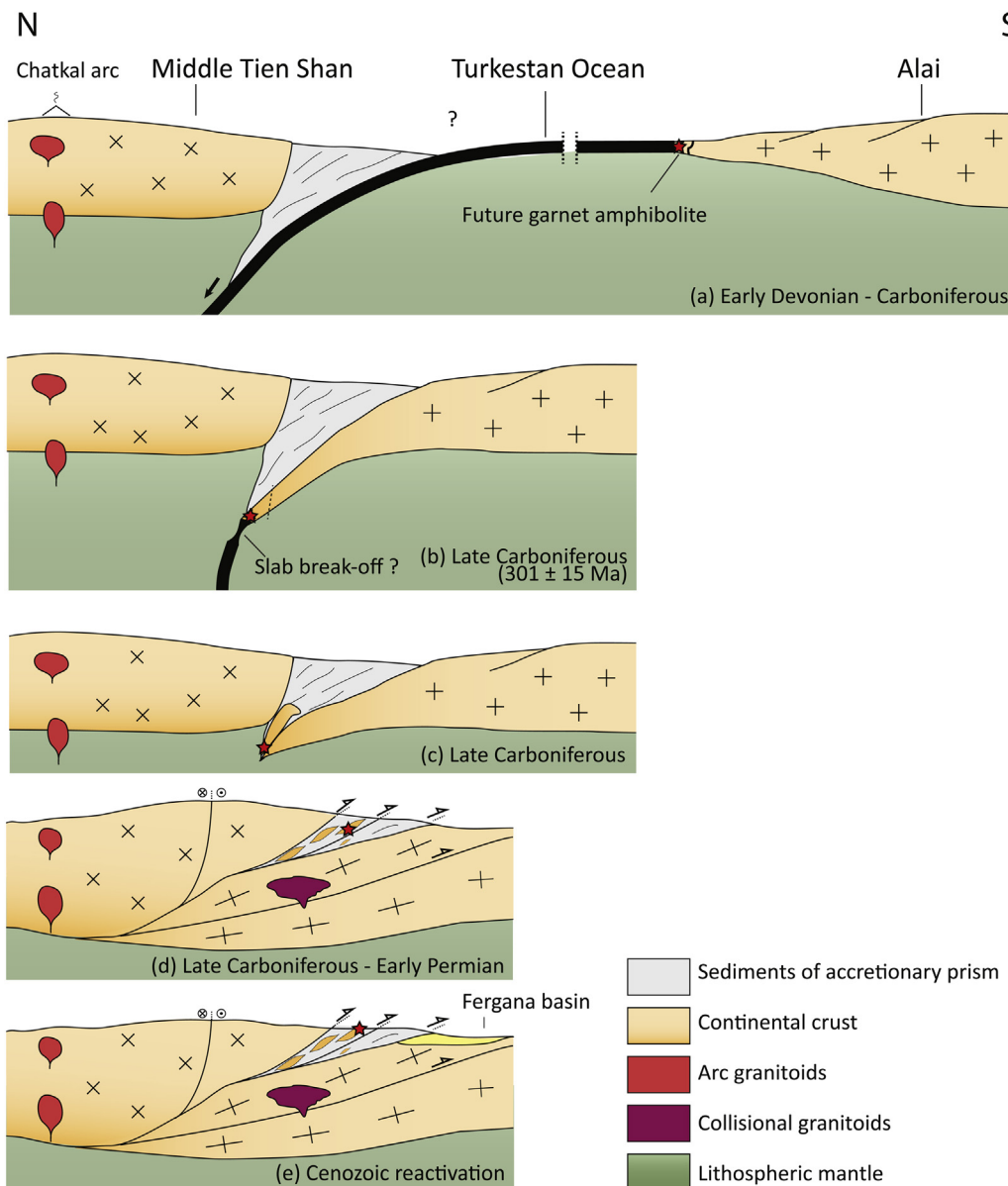


Fig. 10. Model of geodynamic evolution of Middle Tien Shan to the west of the Talas-Fergana fault in Late Paleozoic. Comments in the text (Section 6.2).

Stampfli, 2008; Kröner et al., 2014; Rojas-Agramonte et al., 2014). However, the age of the high-temperature metamorphic stage and partial melting of this former arc unit is still unconstrained. It could be either linked to this Ordovician event or to the collision of the Alai block with the Middle-Tien Shan following the closure of the Turkestan Ocean.

Allanite dating performed in this study gives a first constraint on the age of the HP stage recorded by the garnet amphibolites of the Chatkal range, which is of 301 ± 15 Ma (MSWD = 2.8). The alkaline chemical composition of the garnet amphibolites (retrogressed eclogites) and their geometry of mafic lenses intercalated in micaschists suggest that they could be former alkaline magmatic dykes cross-cutting a tectonically thinned continental margin during a rifting event (OCT, Manatschal and Müntener, 2009). These results suggest that the Turkestan Ocean subduction ended during the Late Carboniferous, when the OCT entered the subduction zone (Fig. 10b). This transition from oceanic subduction to collision is also marked by the end of the magmatic activity in the arc (e.g. Seltmann et al., 2011). The P-T estimates for the HP stage suggest that the OCT was buried at a depth of about 60 km

(assuming a lithostatic pressure of 1 kbar ~ 3.3 km) before its exhumation within the accretionary prism (Fig. 10c). Then, the collision continued and resulted into crustal thickening, characterized by nappe stacking and huge isoclinal vertical folds. Barrovian metamorphic stage (staurolite-bearing schists), partial melting, and granitic magmatism occurred during this collisional stage suggesting that the geothermal gradient increased significantly (Fig. 10d). This stage of collision is responsible for ~ 25 km of vertical ascent of the former eclogite, as suggested by their P-T path showing a low pressure-high temperature retrogression at 7–11 kbar. These HP rocks were exhumed at the back of the suture as suggested by their geographical location tens of kilometers northwest of the suture front. This exhumation path is observed in many orogens such as in the Alps or in the Himalayas (De Sigoyer et al., 2000; Yamato et al., 2008). This complex Late Carboniferous evolution on the western side of the TFF could explain the actual distribution of ophiolites along the South Tien Shan suture (Tursungaziev and Petrov, 2008). These ophiolites are not aligned contrary to the eastern side of TFF, but follow a 'S-shape'. This shape is ascribed to late-collisional post-nappe folding. As a result, it is difficult to

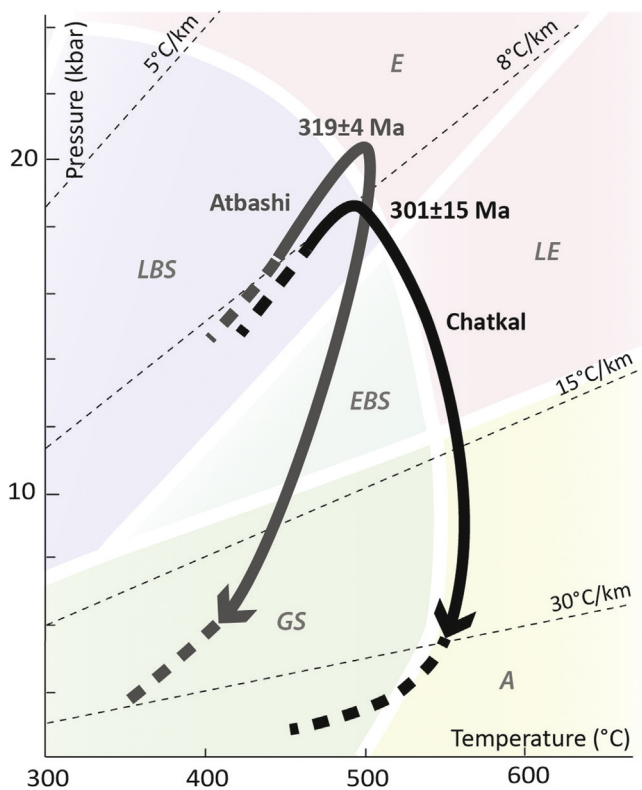


Fig. 11. Comparison of P - T path of HP rocks from the Chatkal range (this study) and from the Atbashi range (after Hegner et al., 2010 and Loury et al., 2015). Black dashed lines are isothermal gradients. Metamorphic facies grid after Evans (1990), abbreviations: GS – greenschist, A – amphibolite, LBS – lawsonite blueschist, EBS – epidote blueschist, LE – lawsonite eclogite, E – eclogite.

constrain the initial position of the subduction front. Later, during the Permian, transcurrent tectonics affected the entire CAOB, resulting in a dextral motion of the TFF mainly at 260–290 Ma (Konopelko et al., 2013; Rolland et al., 2013). Consequently, the total offset of the TFF using the position of the suture could be overestimated.

6.3. Comparison with the Atbashi range eclogites

The P - T - t path obtained for HP rocks from the Chatkal range, to the west of the TFF, can be compared with previously published data from the Atbashi range, to the east of the TFF. Both areas lie along the STSs. Following Loury et al. (2015), we define the STSs as the suture resulting from the collision of the Tarim and Alai block with the South Kazakhstan margin following the Turkestan Ocean closure. It differs from the literature on the Chinese side (e.g., Charvet et al., 2011), where the South-Tien Shan suture term generally refers to the closure of a small back-arc domain to the south of the STSs that we consider.

Considering their P - T conditions, the Chatkal eclogites were exhumed along a relatively warm geothermal gradient ($24^{\circ}\text{C}/\text{km}$) explaining the strong amphibolite facies overprint. On the contrary the eclogites from the Atbashi range were exhumed along a cold geothermal gradient similar to the prograde gradient ($8–10^{\circ}\text{C}/\text{km}$), as shown by slight blueschist facies retrogression (Fig. 11, Loury et al., 2015). This difference of geothermal gradients during the exhumation reflects differences in geological histories.

In the Chatkal range, before its collision with the Alai block, the south margin of the Middle Tien Shan was an active continental margin. Moreover, the collision was marked by nappe-stacking, folding and thickening of the upper plate. Such a collision is

generally characterized by a hot geothermal gradient of $30–40^{\circ}\text{C}/\text{km}$ associated with Barrovian metamorphism and fluid circulation along shear zones (e.g. Le Fort, 1986; Faure et al., 2009). These features increase the kinetics of metamorphic reactions and thus favor the retrogression. The HP rocks of the Chatkal range were thus exhumed in a collisional context that reworked an already ‘hot’ Andean-type active margin, which explains the overprint of the subduction metamorphism by a higher temperature – lower pressure metamorphism. This type of mid- to high-temperature exhumation is described in many areas such as in the Himalayas (Le Fort et al., 1997; Guillot et al., 2008; Lanari et al., 2013), in the European Variscan belt (Mercier et al., 1991; Schulmann et al., 2009) or in the Andes (Riel et al., 2013).

In contrast, to the east of the TFF, in the Atbashi range, the structure of the subduction prism is well-preserved (Loury et al., 2015). The Atbashi range comprises a blueschist-facies accretionary prism unit, overthrust by an ophiolite, itself thrusted by a HP sedimentary unit containing mafic boudins of well-preserved eclogites and then by a continental eclogitic unit exhumed to its south along a detachment. The preservation of this subduction complex and the preservation of eclogites without any high temperature retrogression suggest a rapid exhumation along a cold geothermal gradient up to the surface or sub-surface. This is also supported by a very short age difference between. The HP peak is dated at 319 ± 4 Ma (Sm-Nd whole rock, Hegner et al., 2010) or $323–327$ Ma (^{40}Ar - ^{39}Ar on phengite, Simonov et al., 2008) and the blueschist retrogression is dated at 316 ± 3 Ma (^{40}Ar - ^{39}Ar on phengite, Hegner et al., 2010). The occurrence of eclogite pebbles in conglomerates dated at $295–303$ Ma (Baslakunov et al., 2007) provides minimum age estimation for the final exhumation at the surface. The deformation and metamorphic history are linked to the subduction and subsequent exhumation, but do not feature any collisional nappe-stacking nor any high-temperature metamorphism like in the Chatkal range. Furthermore, the structures indicate a south-dipping subduction in Atbashi (Loury et al., 2015) and a north-dipping subduction in Chatkal. Consequently, the contexts of exhumation of HP rocks are different on both sides of the TFF: subduction stacking to the east and collisional to the west.

Moreover, the age of HP metamorphism appears to be slightly different. Allanite in garnet amphibolites of the Chatkal range yields an age of 301 ± 15 Ma. In the Atbashi range, ages obtained for the HP stage range from 319 ± 4 (Hegner et al., 2010) to $323–327$ Ma (Simonov et al., 2008). If we consider the younger age obtained in Atbashi, the ages for HP stage are the same within errors on both side of the TFF. However, the important error on the age obtained for the Chatkal range and the older ages for the Atbashi range suggest that the HP stage could be slightly younger to the west as compared to the east of the TFF. Consequently, it suggests that the Tarim collided with Kazakhstan 5–20 Ma before the Alai block.

6.4. Implications for the evolution of the South Tien Shan suture in the context of CAOB

On the basis of these new results and previous published works (Filippova et al., 2001; Windley et al., 2007; Biske and Seltmann, 2010), we propose a schematic evolution model for the evolution of the STSs in the Late Paleozoic in the context of CAOB (Fig. 12).

During the Early Carboniferous times (Fig. 12a), the Kazakh microcontinent was surrounded by the Ob-Zaisan, Junggar-Balkhash, Turkestan and Uralian oceans, which were all subducting beneath Kazakhstan. All the continents and microcontinents migrated northward and rotated clockwise (Filippova et al., 2001). The oblique collision between the Tarim and the South Kazakhstan margin leading to the formation of the STSs could have begun in its northernmost part but the age of this collision remains debated

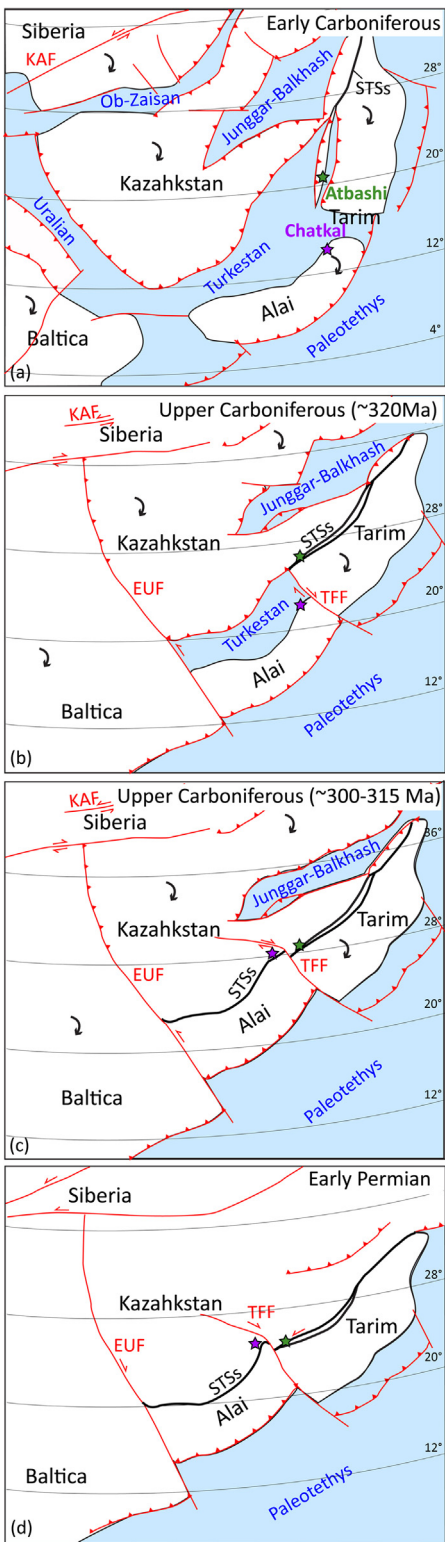


Fig. 12. Schematic tectonic evolution of Central Asia in Late Paleozoic times, modified from Filippova et al. (2001), Heubeck et al. (2001), Loury et al. (2015), Jourdon et al. (this volume). (a) Early Carboniferous, (b) Upper Carboniferous, ~320 Ma, (c) Upper Carboniferous, ~300–315 Ma (d) Early Permian. Comments in the text (see Section 6.4). Red lines represent major strike-slip faults and thrusts or subductions (with red triangles). Bold black line represents the South Tien Shan Suture (STSs). Abbreviations used: EUF – East Urals Fault, KAF – Kuznetsky Alatau Fault, TFF – Talas-Fergana Fault.

(Xiao et al., 1992; Gao and Klemd, 2003; Zhang et al., 2009; Su et al., 2010; Charvet et al., 2011; Li et al., 2011; Liu et al., 2014).

During the *Upper Carboniferous* times, the Uralian and Ob-Zaisan Oceans were closed to the west and north of Kazakhstan, respectively. At c. 320 Ma (Fig. 12b), the Turkestan Ocean continued to close with the collision between the Tarim and the South Kazakh margin extending the STSs toward the southwest. The HP rocks from the Atbashi range were formed at that time (Simonov et al., 2008; Hegner et al., 2010). The Tarim craton was entirely accreted to the Kazakhstan but a part of the Turkestan Ocean probably remained open to the west between the Alai block and the Kazakh margin. It led to the activation of the TFF as a transform fault between the Tarim craton and the Alai block. This is in agreement with the minimum initiation age of the TFF constrained at 312 ± 4 Ma by $^{40}\text{Ar}/^{39}\text{Ar}$ on muscovite in mylonites (Rolland et al., 2013). Around 5–20 Ma later (Fig. 12c), the Alai block collided with the South-West margin of Kazakhstan, prolonging the STSs toward the southwest. This study provides a first estimation for the age of this collision but it remains to be refined. The HP rocks of the Chatkal range were probably exhumed rapidly after 300 Ma. This collision led to nappe-stacking, crustal thickening and Barrovian metamorphism during which the eclogites were retrogressed. The TFF propagated inside the continent toward the north-west and joined an older early Paleozoic fault corresponding to the boundary between the Kyrgyz North and Middle Tien Shan (Nikolaev, 1933).

In the *Early Permian* times (Fig. 12d), all the Oceans were closed and the continents were amalgamated. The Junggar-Balkhash Ocean was closed in the Late Carboniferous or Early Permian (Charvet et al., 2011). Paleomagnetic data indicates a strong decrease of northward drifting and clockwise rotation of amalgamated continents (Didenko, 1997; Filippova et al., 2001). A general transcurrent tectonic context affected the CAOB, which evolved as a single continental block (e.g. Suvorov, 1968; Burtman, 1980; Buslov et al., 2004). For example, in the Tien Shan, the TFF began to offset the STSs, the major offset of which occurred at 260–290 Ma (Rolland et al., 2013).

7. Conclusion

In this study, we present new petrochronological data for highly retrogressed HP rocks in the Chatkal range. A micro-mapping approach was used to decipher the *P-T* path of garnet amphibolites (retrogressed eclogites) from the pressure peak to the late stages of exhumation. The micro-mapping allowed to extract local chemical compositions to calculate a local effective bulk composition used for *P-T* section calculation. This forward modeling approach was combined with thousands of *P-T* estimates obtained with empirical and semi-empirical thermobarometry applied to the maps. The results show a HP peak at 490 ± 50 °C and 18.5 ± 2 kbar. Two exhumation stages were preserved, at a constant temperature of 560 ± 50 °C and decreasing pressure from 11 to 7 kbar implying an exhumation along a relatively hot geothermal gradient (~ 24 °C/km). These petrological data were complemented with allanite geochronology in order to date the HP stage. Allanite grains associated with the HP mineral assemblages yield a Late Carboniferous age of 301 ± 15 Ma for the metamorphic peak which is 5–20 Ma younger than the age of HP metamorphism east of the TFF.

These data allow us to improve the understanding of the geo-dynamic evolution of South Tien Shan to the west of the TFF. The northward subduction of Turkestan Ocean ended around 300 Ma, when the thin continental margin entered in subduction. HP rocks corresponding to this stage were then exhumed in a collisional setting, in which they were retrogressed into garnet amphibolites. These results highlight some significant differences for the South Tien Shan evolution on both sides of the TFF:

The contexts of exhumation of HP rocks are different, with subduction stacking to the east and collision to the west.

To the west, the north-dipping subduction and subsequent collision with the arc generated strong folding, crustal thickening and regional Barrovian metamorphism.

This collisional phase considerably deformed the suture making it difficult to decipher the initial position of the subduction front, while the collisional phase is less developed to the east of the TFF.

To the east, the Turkestan Ocean closure ended around 320 Ma when the Tarim craton collided with the Kazakhstan microcontinent, while to the west, a branch of the Turkestan Ocean probably remained open at that time. Final closure of the remaining oceanic basin occurred around 300 Ma when the Alai block collided with the Kazakhstan microcontinent. However this timing remains to be refined, as the error on the age obtained for the HP stage in the Chatkal range is too important to fully distinct differences in the HP stage age on both sides of the fault.

Finally, this study shows that the use of a micro-mapping approach combined with in situ geochronology is highly relevant to study retrogressed eclogites. The understanding of this kind of rocks is important to reconstruct the history of orogens as they generally are the marker of the subduction-collision transition.

Acknowledgements

This work was supported by the DARIUS Program and the project DSP-Tibet funded by the Agence Nationale de la Recherche (ANR-13-BS06-012-01). The authors warmly thank the help and support of M.F. Brunet and E. Barrier for the coordination of this project and the organization of related workshops. We appreciate the help of A.K. Rybin, Director of the Research Station of the Russian Academy of Sciences in Bishkek, for help with logistics and organizational support. We acknowledge O. Bruguier for his assistance during the LA-ICPMS analyses and V. Magnin for her assistance during micro-probe analyses. In addition, we thank, we thank D. Alexeiev for constructive discussions. This paper was significantly enhanced following the careful reviews of M. Poujol and an anonymous reviewer and editorial comments of P. Yamato and W. Schellart.

References

- Agard, P., Yamato, P., Jolivet, L., Burov, E., 2009. Exhumation of oceanic blueschists and eclogites in subduction zones: timing and mechanisms. *Earth Sci. Rev.* 92, 53–79, <http://dx.doi.org/10.1016/j.earscirev.2008.11.002>
- Alekseev, D.V., Degtyarev, K.E., Kotov, A.B., Sal'nikova, E.B., Tretyakov, A.A., Yakovleva, S.Z., Anisimova, I.V., Shatagin, K.N., 2009b. Late Paleozoic subductional and collisional igneous complexes in the Naryn segment of the Middle Tien Shan (Kyrgyzstan). *Dokl. Earth Sci.* 427, 760–763, <http://dx.doi.org/10.1134/S1028334X09050122>
- Alexeiev, D.V., Cook, H.E., Buvtyshkin, V.M., Golub, L.Y., 2009a. Structural evolution of the Ural–Tian Shan junction: a view from Karatau ridge, South Kazakhstan. *C. R. Geosci.* 341, 287–297, <http://dx.doi.org/10.1016/j.crte.2008.12.004>
- Alexeiev, D.V., Ryzantsev, A.V., Kröner, A., Tretyakov, A., Xia, A.X., Liu, D.Y., 2011. Geochemical data and zircon ages for rocks in a high-pressure belt of Chu-Yili Mountains, southern Kazakhstan: implications for the earliest stages of accretion in Kazakhstan and the Tianshan. *J. Asian Earth Sci.* 42, 805–820.
- Alexeiev, D.V., Biske, Y.S., Wang, B., Djenchuraeva, A., Getman, V., Aristov, O.F., Kröner, V.A., Liu, A.H., Zhong, L., 2015a. Tectono-Stratigraphic framework and Palaeozoic evolution of the Chinese South Tianshan. *Geotectonics* 49, 93–122, <http://dx.doi.org/10.1134/S0016852115020028>
- Alexeiev, D.V., Cook, H.E., Djenchuraeva, A.V., Mikolaichuk, A.V., 2015b. The stratigraphic, sedimentologic and structural evolution of the southern margin of the Kazakhstan continent in the Tien Shan Range during the Devonian to Permian. In: Brunet, M.F., McCann, T., Sobel, E.R. (Eds.), *Geological Evolution of Central Asian Basins and the Tien-Shan Range*. Geological Society of London Special Publication (in press).
- Allen, M.B., Vincent, S.J., 1997. Fault reactivation in the Junggar region, northwest China: the role of basement structures during Mesozoic – Cenozoic compression. *J. Geol. Soc. London* 154, 151–155.
- Allen, M.B., Alsop, G.I., Zhemchuzhnikov, V.G., 2001. Dome and basin refolding and transpressive inversion along the Karatau Fault System, southern Kazakhstan. *J. Geol. Soc. London* 158, 83–95.
- Avdeev, A.V., Kovalev, A.A., 1989. *Ophiolites and Evolution of the Southwestern Part of the Ural–Mongolia Folded Belt* (in Russian).
- Bakirov, A.B., 1978. *Tectonic Position of Metamorphic Complexes in Tianshan. Frunze III* (in Russian).
- Bakirov, A.B., Kiselev, V.V., Ivleva, E.A., Lukashova, E.M., 1996. On the age of the Kasan metamorphic complex. *An Resp. Kyrg. 1*, 31–37.
- Bakirov, A.B., Kotov, V.V., 1988. Eclogite-bearing metamorphic complexes as indicator of the ancient continent collision zone (in Russian). In: *Precambrian and Lower Paleozoic of Tianshan*, pp. 4–25.
- Bakirov, A.B., Maksumova, R.A., 2001. Geodynamic evolution of the Tien Shan lithosphere. *Russ. Geol. Geophys.* 42, 1359–1366.
- Bakirov, A.B., Tagiri, M., Sakiev, K.S., Ivleva, E.A., 2003. The lower Precambrian rocks in the Tien Shan and their geodynamic setting. *Geotectonics* (English Transl.) 5, 27–40.
- Baslakunov, J., Takasu, A., Tagiri, M., Bakirov, A., Sakiev, K., 2007. Two modes of occurrence of eclogites from the Altaby Range, southern Tien-Shan, Kyrgyzstan. In: American Geophysical Union Fall Meeting, Abstract V41C0730B.
- Berger, A., Bousquet, R., 2008. Subduction-related metamorphism in the Alps: review of isotopic ages based on petrology and their geodynamic consequences. *Geol. Soc. London Spec. Publ.* 298, 117–144.
- Berman, R.G., 1988. Internally-consistent thermodynamic data for minerals in the system $\text{Na}_2\text{O}-\text{K}_2\text{O}-\text{CaO}-\text{MgO}-\text{FeO}-\text{Fe}_2\text{O}_3-\text{Al}_2\text{O}_3-\text{SiO}_2-\text{TiO}_2-\text{H}_2\text{O}-\text{CO}_2$. *J. Petrol.* 29, 445–522.
- Biske, Y.S., 1995. Late Paleozoic collision of Kirghiz-Kazakhstan and Tarim paleocontinents. *Geotectonics* 1, 31–39.
- Biske, Y.S., 1996. *Paleozoic Structure and History of South Tian-Shan. Sankt-Pete, St.-Petersburg* (in Russian).
- Biske, Y.S., Seltmann, R., 2010. Paleozoic Tian-Shan as a transitional region between the Rheic and Urals-Turkestan oceans. *Gondwana Res.* 17, 602–613, <http://dx.doi.org/10.1016/j.gr.2009.11.014>
- Brown, M., 1993. *P–T–t evolution of orogenic belts and the causes of regional metamorphism*. *J. Geol. Soc.* 150 (2), 227–241.
- Burtman, B.S., 2006. The Tien Shan early paleozoic tectonics and geodynamics. *Russ. J. Earth Sci.* 8, 1–23, <http://dx.doi.org/10.2205/2006ES000202>
- Burtman, V.S., 1964. *Talas–Fergana strike-slip fault (Tien Shan)*. *Geol. Inst. Acad. Sci. USSR, Trans. Moscow, "Nauka"* 104, 143p. (in Russian).
- Burtman, V.S., 1975. *Structural geology of Variscan Tien Shan*. *USSR. Am. J. Sci.* 275-A, 157–186.
- Burtman, V.S., 1980. *Faults of middle Asia*. *Am. J. Sci.* 280, 725–744.
- Buslov, M.M., Fujiwara, Y., Iwata, K., Semakov, N.N., 2004. Late paleozoic-early mesozoic geodynamics of central Asia. *Gondwana Res.* 7, 791–808.
- Carignan, J., Hild, P., Mevelle, G., Morel, J., Yeghicheyan, D., 2001. Routine analyses of trace elements in geological samples using flow injection and low pressure on-line liquid chromatography coupled to ICP-MS: a study of geochemical reference materials BR, DR-N, UB-N, AN-G and GH. *Geostand. Newsl.* 25, 187–198, <http://dx.doi.org/10.1111/j.1751-908X.2001.tb00595.x>
- Cenki-Tok, B., Darling, J.R., Rolland, Y., Dhuime, B., Storey, C.D., 2014. Direct dating of mid-crustal shear zones with synkinematic allanite: new in situ U–Th–Pb geochronological approaches applied to the Mont Blanc massif. *Terra Nova* 26, 29–37, <http://dx.doi.org/10.1111/ter.12066>
- Cenki-Tok, B., Oliot, E., Rubatto, D., Berger, A., Engi, M., Janots, E., Thomsen, T.B., Manzotti, P., Regis, D., Spandler, C., Robyr, M., Goncalves, P., 2011. Preservation of Permian allanite within an Alpine eclogite facies shear zone at Mt Mucrone, Italy: mechanical and chemical behavior of allanite during mylonitization. *Lithos* 125, 40–50.
- Charvet, J., Shu, L., Laurent-Charvet, S., Wang, B., Faure, M., Cluzel, D., Chen, Y., Jong, K., 2011. Palaeozoic tectonic evolution of the Tianshan belt, NW China. *Sci. China Earth Sci.* 54, 166–184, <http://dx.doi.org/10.1007/s11430-010-4138-1>
- Coleman, G., 1989. Continental growth of northwest China. *Tectonics* 8, 621–635.
- Cook, H.E., Zhemchuzhnikov, V.G., Zempolich, W.G., Buvtyshkin, V.M., Zhaimina, V.Y., Kotova, E.A., Golub, L.Y., Zorin, A.Y., Lehmann, P.J., Alexeiev, D.V., Giovannelli, A., Viaggi, M., Fretwell, N., Lapointe, P., Corboy, J.J., Bowman, M., De Coo, J.C.M., 2002. *Devonian and Carboniferous carbonate platform facies in the Bolshoi Karatau, Southern Kazakhstan: outcrop analogs for coeval carbonate oil and gas fields in the North Caspian basin, western Kazakhstan*. In: Zempolich, W.G., Cook, H.E. (Eds.), *Paleozoic Carbonates of the Commonwealth of the Independent States (CIS): Subsurface Reservoirs and Outcrop Analogs*. Society for Sedimentary Geology (SEPM), pp. 81–122.
- Dale, J., Holland, T., Powell, R., 2000. Hornblende-garnet-plagioclase thermobarometry: a natural assemblage calibration of the thermodynamics of hornblende. *Contrib. Mineral. Petro.* 140, 353–362.
- Darling, J.R., Storey, C.D., Engi, M., 2012. Allanite U–Th–Pb geochronology by laser ablation ICPMS. *Chem. Geol.* 292–293, 103–115, <http://dx.doi.org/10.1016/j.chemgeo.2011.11.012>
- De Andrade, V., 2006. *De l'imagerie chimique à la micro-cartographie Pression-Température-Déformation: évolution minéralogique et transport de matière dans des systèmes en déséquilibre thermomécanique*. Ph.D. thesis, Université Joseph Fourier-Grenoble I.
- De Capitani, C., Petrakakis, K., 2010. The computation of equilibrium assemblage diagrams with Theriax/Domino software. *Am. Mineral.* 95, 1006–1016, <http://dx.doi.org/10.2138/am.2010.3354>
- De Grave, J., Glorie, S., Ryabinin, A., Zhimulev, F., Buslov, M.M., Izmer, A., Elburg, M., Vanhaecke, F., Van den haute, P., 2012. Late Palaeozoic and Meso-Cenozoic tectonic evolution of the southern Kyrgyz Tien Shan: Constraints from

- multi-method thermochronology in the Trans-Alai, Turkestan-Alai segment and the southeastern Fergana Basin. *J. Asian Earth Sci.* 44, 149–168, <http://dx.doi.org/10.1016/j.jseas.2011.04.019>
- Degtyarev, K.E., 2012. *Tectonic Evolution of the Early Paleozoic Island Arcs and Continental Crust Formation in the Caledonides of Kazakhstan*, Geological Institute, Russian Academy of Sciences, Transactions, 602 (in Russian). Geos Publishing House, Moscow.
- De Sigoyer, J., Chavagnac, V., Blichert-Toft, J., Villa, I., Luais, B., Guillot, S., Cosca, M., Mascle, G., 2000. *Dating the Indian continental subduction and collisional thickening in the northwest Himalaya: multichronology of the Tso Morari eclogites*. *Geology* 28, 487–490.
- Didenko, A., abstract of Ph. D. thesis, Moscow 1997. *Paleomagnetism and Geodynamic Evolution of the Urals–Mongolia foldbelt* (in Russian).
- Duchene, S., Blichert-Toft, J., Luais, B., Telouk, P., Lardeaux, J.M., Albareda, F., Duchêne, S., Blichert-Toft, J., Luais, B., Telouk, P., Lardeaux, J.M., Albareda, F., 1997. *The Lu–Hf dating of garnets and the ages of the Alpine high-pressure metamorphism*. *Nature* 387, 3–6.
- Eganov, E.A., Sovetov, Y.K., 1979. *Karatau – A Model for Phosphorite Deposition*. The Institute of Geology and Geophysics Ac. Sci USSR, Transactions, Issue 427. Nauka, Novosibirsk.
- Evans, B., 1990. *Phase relations of epidote-blueschists*. *Lithos* 25, 3–23.
- Faure, M., Lardeaux, J.M., Ledru, P., 2009. *A review of the pre-Permian geology of the Variscan French Massif Central*. *C. R. Geosci.* 341, 202–213.
- Filippova, I.B., Bush, V.A., Didenko, A.N., 2001. *Middle Paleozoic subduction belts: the leading factor in the formation of the Central Asian fold-and-thrust belt*. *Russ. J. Earth Sci.* 3, 405–426.
- Galitskiy, V.V., 1967. *Tectonics of Karatau range (South Kazakhstan)*. In: *Tectonics and Dynamo-Metamorphism of the Kazakhstan Paleozoides* (in Russian). 'Nauka' Institute of Geological Sciences, Alma-Ata, pp. 3–47.
- Gao, J., Klemd, R., 2003. Formation of HP–LT rocks and their tectonic implications in the western Tianshan Orogen, NW China: geochemical and age constraints. *Lithos* 66, 1–22, [http://dx.doi.org/10.1016/S0024-4937\(02\)00153-6](http://dx.doi.org/10.1016/S0024-4937(02)00153-6)
- Ge, R., Zhu, W., Wu, H., Zheng, B., Zhu, X., He, J., 2012. The Paleozoic northern margin of the Tarim Craton: passive or active? *Lithos* 142–143, 1–15, <http://dx.doi.org/10.1016/j.lithos.2012.02.010>
- Ghes, M.D., 2008. *Terrane Structure and Geodynamic Evolution of the Caledonides of the Tian Shan*. Altyn Tamga Publishing House, Bishkek (in Russian).
- Giere, R., Sorensen, S.S., 2004. Allanite and other REE-rich epidote-group minerals. *Rev. Mineral. Geochem.* 56, 431–493.
- Glorie, S., De Grave, J., Buslov, M.M., Zhimulev, F.I., Stockli, D.F., Batalev, V.Y., Izmer, A., Van Den Haute, P., Vanhaecke, F., Elburg, M.A., 2011. Tectonic history of the Kyrgyz South Tien Shan (Atbashi-Inylchek) suture zone: the role of inherited structures during deformation-propagation. *Tectonics* 30, TC6016, <http://dx.doi.org/10.1029/2011TC002949>
- Gregory, C.J., Rubatto, D., Allen, C.M., Williams, I.S., Hermann, J., Ireland, T., 2007. *Allanite micro-geochronology: a LA-ICP-MS and SHRIMP U–Th–Pb study*. *Chem. Geol.* 245, 162–182.
- Guillot, S., Mahéo, G., de Sigoyer, J., Hattori, K.H., Pécher, A., 2008. Tethyan and Indian subduction viewed from the Himalayan high- to ultrahigh-pressure metamorphic rocks. *Tectonophysics* 451, 225–241, <http://dx.doi.org/10.1016/j.tecto.2007.11.059>
- Hacker, B.R., Wang, Q., 1995. *Ar–Ar geochronology of ultrahigh pressure metamorphism in central China*. *Tectonics* 14, 994–1006.
- Hegner, E., Klemd, R., Kröner, A., Corsini, M., Alexeev, D.V., Iaccheri, L.M., Zack, T., Dulski, P., Xia, X., Windley, B.F., 2010. Mineral ages and *P–T* conditions of Late Paleozoic high-pressure eclogite and provenance of melange sediments from Atbashi in the south Tianshan orogen of Kyrgyzstan. *Am. J. Sci.* 310, 916–950, <http://dx.doi.org/10.2475/09.2010.07>
- Heubeck, C., 2001. *Assembly of Central Asia during the middle and late Paleozoic*. In: Hendrix, M.S., Davis, G.A. (Eds.), *Paleozoic and Mesozoic Tectonic Evolution of Central Asia: From Continental Assembly to Intracontinental Deformation*, vol. 194. Memoir Geological Society of America, pp. 1–22.
- Hermann, J., 2002. Allanite: thorium and light rare earth element carrier in subducted crust. *Chem. Geol.* 192, 289–306, [http://dx.doi.org/10.1016/S0009-2541\(02\)00222-X](http://dx.doi.org/10.1016/S0009-2541(02)00222-X)
- Holland, T.J.B., 1983. The experimental determination of activities in disordered and short-range ordered jadeitic pyroxenes. *Contrib. Mineral. Petro.* 82, 214–220, <http://dx.doi.org/10.1007/BF01166616>
- Holland, T.J.B., 1990. Activities of components in omphacitic solid solutions – An application of Landau theory to mixtures. *Contrib. Mineral. Petro.* 105, 446–453.
- Holland, T.J.B., Blundy, J., 1994. Non-ideal interactions in calcic amphiboles and their bearing on amphibole-plagioclase thermometry. *Contrib. Mineral. Petro.* 116, 433–447, <http://dx.doi.org/10.1007/BF00310910>
- Hunziker, P., 2003. *The Stability of Tri-octahedral Fe²⁺-Mg–Al Chlorite: A Combined Experimental and Theoretical Study*. PhD thesis, Mineralog.–Petrogr. Inst. Uni Basel.
- Jackson, S.E., Pearson, N.J., Griffin, W.L., Belousova, E.A., 2004. *The application of laser ablation-inductively coupled plasma mass spectrometry to in situ U–Pb zircon geochronology*. *Chem. Geol.* 211, 47–69.
- Janots, E., Engi, M., Rubatto, D., Berger, A., Gregory, C., Rahn, M., 2009. Metamorphic rates in collisional orogeny from in situ allanite and monazite dating. *Geology* 37, 11–14, <http://dx.doi.org/10.1130/G25192A.1>
- Janots, E., Rubatto, D., 2014. U–Th–Pb dating of collision in the external Alpine domains (Urseren zone, Switzerland) using low temperature allanite and monazite. *Lithos* 184–187, 155–166.
- Jolivet, L., Huchon, P., Rangin, C., 1989. *Tectonic setting of Western Pacific marginal basins*. *Tectonophysics*.
- Jourdon, A., Petit, C., Rolland, Y., Loury, C., Bellahsen, N., Guillot, S., Ganino, C., Mikolaichuk, A.V., 2015. From subduction to collision, the Paleozoic accretionary history of the Tien Shan (Central Asian Orogenic Belt): insight from new structural data (Kyrgyzstan). *J. Geodyn.* (this volume).
- Keller, L.M., de Capitani, C., Abart, R., 2005. A quaternary solution model for white micas based on natural coexisting phengite-paragonite pairs. *J. Petrol.* 46, 2129–2144, <http://dx.doi.org/10.1093/petrology/egi050>
- Khrustov, Y.V., Mikolaichuk, A.V., 1983. *Geosynclinal basement of the crust of the Fergana-Koksha Hercynides*. *Geotectonics* 17, 233–241.
- Kiselev, V.V., Apayarov, F.K., Komartsev, V.T., Tsyanok, E.N., Lukashova, E.M., 1993. *Isotopic ages of zircons from crystalline complexes of the Tianshan*. In: Kozakov, I.K. (Ed.), *Early Precambrian of the Central Asia Folded Belt*. St-Petersburg, pp. 99–115.
- Konopelko, D., Biske, G., Seltmann, R., Kiseleva, M., Matukov, D., Sergeev, S., 2008. Deciphering Caledonian events: timing and geochemistry of the Caledonian magmatic arc in the Kyrgyz Tien Shan. *J. Asian Earth Sci.* 32, 131–141, <http://dx.doi.org/10.1016/j.jseas.2007.10.017>
- Konopelko, D., Seltmann, R., Apayarov, F., Belousova, E., Izokh, A., Lepikhina, E., 2013. U–Pb–Hf zircon study of two mylonitic granite complexes in the Talas–Fergana fault zone, Kyrgyzstan, and Ar–Ar age of deformations along the fault. *J. Asian Earth Sci.* 73, 334–346, <http://dx.doi.org/10.1016/j.jseas.2013.04.046>
- Kröner, A., Alexeev, D.V., Hegner, E., Rojas-Agramonte, Y., Corsini, M., Chao, Y., Wong, J., Windley, B.F., Liu, D., Tretyakov, A.A., 2012. Zircon and muscovite ages, geochemistry, and Nd–Hf isotopes for the Aktyuz metamorphic terrane: Evidence for an Early Ordovician collisional belt in the northern Tianshan of Kyrgyzstan. *Gondwana Res.* 21, 901–927, <http://dx.doi.org/10.1016/j.gr.2011.05.010>
- Kröner, A., Alexeev, D.V., Rojas-Agramonte, Y., Hegner, E., Belousova, E., Mikolaichuk, A.V., Seltmann, R., Liu, D., Kiselev, V.V., 2013. Mesoproterozoic (Grenville-age) terranes in the Kyrgyz North Tianshan: Zircon ages and Nd–Hf isotopic constraints on the origin and evolution of basement blocks in the southern Central Asian Orogen. *Gondwana Res.* 23, 272–295, <http://dx.doi.org/10.1016/j.gr.2012.05.004>
- Kröner, A., Kovach, V., Belousova, E., Hegner, E., Armstrong, R., Dolgopolova, A., Seltmann, R., Alexeev, D.V., Hoffmann, J.E., Wong, J., Sun, M., Cai, K., Wang, T., Tong, Y., Wilde, S.A., Degtyarev, K.E., Rytsk, E., 2014. Reassessment of continental growth during the accretionary history of the Central Asian Orogenic Belt. *Gondwana Res.* 25, 103–125, <http://dx.doi.org/10.1016/j.gr.2012.12.023>
- Lanari, P., Guillot, S., Schwartz, S., Vidal, O., Tricart, P., Riel, N., Beyssac, O., 2012. Diachronous evolution of the alpine continental subduction wedge: evidence from *P–T* estimates in the Briançonnais Zone houillère (France – Western Alps). *J. Geodyn.* 56–57, 39–54, <http://dx.doi.org/10.1016/j.jog.2011.09.006>
- Lanari, P., Riel, N., Guillot, S., Vidal, O., Schwartz, S., Pecher, A., Hattori, K.H., 2013. Deciphering high-pressure metamorphism in collisional context using microprobe mapping methods: application to the Stak eclogitic massif (northwest Himalaya). *Geology* 41, 111–114, <http://dx.doi.org/10.1130/G35323.1>
- Lanari, P., Vidal, O., De Andrade, V., Dubacq, B., Lewin, E., Grosch, E.G., Schwartz, S., 2014. XMapTools: a MATLAB®-based program for electron microprobe X-ray image processing and geothermobarometry. *Comput. Geosci.* 62, 227–240, <http://dx.doi.org/10.1016/j.cageo.2013.08.010>
- Laurent-Charvet, S., Charvet, J., Monié, P., Shu, L., 2003. *Late Paleozoic strike-slip shear zones in eastern Central Asia (NW China): new structural and geochronological data*. *Tectonics*, 22.
- Le Fort, P., 1986. Metamorphism and magmatism during the Himalayan collision. *Geol. Soc. London, Spec. Publ.* 19, 159–172.
- Le Fort, P., Guillot, S., Pécher, A., 1997. HP metamorphic belt along the Indus suture zone of NW Himalaya: new discoveries and significance. *Comptes Rendus l'Académie des Sci. Earth Planet. Sci.* 325, 773–778.
- Leake, B.E., 1978. *Nomenclature of amphiboles*. *Am. Mineral.* 63, 1023–1052.
- Li, Q., Lin, W., Su, W., Li, X., Shi, Y., Liu, Y., Tang, G., 2011. SIMS U–Pb rutile age of low-temperature eclogites from southwestern Chinese Tianshan, NW China. *Lithos* 122, 76–86, <http://dx.doi.org/10.1016/j.lithos.2010.11.007>
- Liu, X., Su, W., Gao, J., Li, J., Jiang, T., Zhang, X., Ge, X., 2014. Paleozoic subduction erosion involving accretionary wedge sediments in the South Tianshan Orogen: evidence from geochronological and geochemical studies on eclogites and their host metasediments. *Lithos* 210–211, 89–110, <http://dx.doi.org/10.1016/j.lithos.2014.09.017>
- Lomize, M.G., Demina, L.I., Zarshchikov, A.V., 1997. *The Kyrgyz-Terskei Paleoceanic Basin, Tien Shan*. *Geotectonics* 31, 463–482.
- Loury, C., Rolland, Y., Guillot, S., Mikolaichuk, A.V., Lanari, P., Bruguer, O., Bosch, D., 2015. Crustal-scale structure of South Tien Shan: implications for subduction polarity and Cenozoic reactivation. *Geol. Soc. London, Spec. Publ.* 427, <http://dx.doi.org/10.1144/SP427.4>
- Ludwig, K.R., 2003. *Isoplots 3.00 a geochronological toolkit for Microsoft Excel*. Berkley Geochronol. Cent. Spec. Publ., 4.
- Makarov, V.I., Alekseev, D.V., Batalev, V.Y., Bataleva, E.A., Belyaev, I.V., Bragin, V.D., Dergunov, N.T., Efimova, N.N., Leonov, M.G., Munirova, L.M., Pavlenkin, A.D., Roecker, S., Roslov, Y.V., Rybin, A.K., Shchelochkov, G.G., 2010. Underthrusting of Tarim beneath the Tien Shan and deep structure of their junction zone: Main results of seismic experiment along MANAS Profile Kashgar–Song-Köl. *Geotectonics* 44, 102–126, <http://dx.doi.org/10.1134/S0016852110020020>

- Maksumova, R.A., Dzhenchurava, A.V., Berezanskii, A.V., 2001. Structure and evolution of the Tien Shan nappe-folded orogen. *Geol. I Geofiz.* 42, 1444–1452.
- Manatschal, G., Müntener, O., 2009. A type sequence across an ancient magma-poor ocean-continent transition: the example of the western Alpine Tethys ophiolites. *Tectonophysics* 473, 4–19, <http://dx.doi.org/10.1016/j.tecto.2008.07.021>
- Mercier, L., Lardeaux, J.-M., Davy, P., 1991. On the tectonic significance of retrograde $P-T$ -t paths in eclogites of the French Massif Central. *Tectonics* 10, 131.
- Meyre, C., de Capitani, C., Partzsch, J.H., 1997. A ternary solid solution model for omphacite and its application to geothermobarometry of eclogites from the Middle Adula nappe (Central Alps, Switzerland). *J. Metamorph. Geol.* 15, 687–700.
- Mikolaichuk, A.V., Kurenkov, S.A., Degtyarev, K.E., Rubstov, V.I., 1997. Northern Tianshan, main stages of geodynamic evolution in the late Precambrian and early Paleozoic. *Geotectonics* 31, 445–462.
- Nikolaev, V.A., 1933. About principal structure line of Tianshan. *Proc. All Russ. Mineral. Soc. Ser. 262*, 347–354 (in Russian).
- Osmontbetov, K.O., 1982. Stratified and Intrusive Formations of Kirgiziya, Book 1. Ilim, Frun.
- Parrish, R.R., Gough, S.J., Searle, M.P., Waters, D.J., 2006. Plate velocity exhumation of ultrahigh-pressure eclogites in the Pakistan Himalaya. *Geology* 34, 989, <http://dx.doi.org/10.1130/G22796A.1>
- Peacock, S.M., 1996. Thermal and petrologic structure of subduction zones. In: *Subduction From Top to Bottom*. AGU Geophysical Monograph, pp. 119–133.
- Pearce, J.A., Peate, D.W., 1995. Tectonic implications of the composition of volcanic arc magmas. *Annu. Rev. Earth Planet. Sci.* 23, 251–285.
- Ravna, E.J., 2000. The garnet – clinopyroxene Fe^{2+} – Mg geothermometer: an updated calibration. *Science* (80) 18, 211–219.
- Regis, D., Rubatto, D., Darling, J., Zucali, M., Engi, M., 2014. Multiple metamorphic stages within an eclogite-facies Terrane (Sesia Zone, Western Alps) revealed by Th–U–Pb petrochronology. *J. Petrol.* 55, 1429–1456, <http://dx.doi.org/10.1093/petrology/egu029>
- Riel, N., Hattori, K.H., Guillot, S., Rayner, N., Davis, B., Latif, M., Kausar, A.B., 2008. SHRIMP zircon ages of eclogites in the Stak massif, northern Pakistan. *Himal. J. Sci.* 5, 119–120.
- Riel, N., Guillot, S., Jaillard, E., Martelat, J.E., Paquette, J.L., Schwartz, S., Goncalves, P., Duclaux, G., Thebaud, N., Lanari, P., Janots, E., Yuquilema, J., 2013. Metamorphic and geochronological study of the Triassic El Oro metamorphic complex, Ecuador: Implications for high-temperature metamorphism in a forearc zone. *Lithos* 156–159, 41–68.
- Rojas-Agramonte, Y., Kröner, A., Alexeev, D.V., Jeffreys, T., Khudoley, A.K., Wong, J., Geng, H., Shu, L., Semiletkin, S.A., Mikolaichuk, A.V., Kiselev, V.V., Yang, J., Seltmann, R., 2014. Detrital and igneous zircon ages for supracrustal rocks of the Kyrgyz Tianshan and palaeogeographic implications. *Gondwana Res.* 26, 957–974, <http://dx.doi.org/10.1016/j.gr.2013.09.005>
- Rolland, Y., Alexeev, D.V., Kröner, A., Corsini, M., Loury, C., Monié, P., 2013. Late Palaeozoic to Mesozoic kinematic history of Talas-Ferghana strike-slip Fault (Kyrgyz West Tianshan) revealed by a structural study and 40Ar/39Ar dating. *J. Asian Earth Sci.* 67/68, 76–92, <http://dx.doi.org/10.1016/j.jseas.2013.02.012>
- Rubatto, D., Hermann, J., 2001. Exhumation as fast as subduction? *Geology* 29, 3–6, [http://dx.doi.org/10.1130/0091-7613\(2001\)029<0003:EAFA>2.0.CO;2](http://dx.doi.org/10.1130/0091-7613(2001)029<0003:EAFA>2.0.CO;2)
- Schneider, J., Bosch, D., Monié, P., 2008. Individualization of textural and reactional microdomains in eclogites from the Bergen Arcs (Norway): consequences for Rb/Sr and Ar/Ar radiochronometer behavior during polymetamorphism. *Geochem. Geophys. Geosyst.* 9, Q12001.
- Schulmann, K., Konopásek, J., Janoušek, V., Lexa, O., Lardeaux, J.M., Edel, J.B., Štípká, P., Ulrich, S., 2009. An Andean type Palaeozoic convergence in the Bohemian Massif. *C. R. Geosci.* 341, 266–286.
- Seliverstov, K.V., Ghes, M.D., 2001. Petrochemical features of magmatic rocks and main characteristics of middle carboniferous – early Permian subduction. *Russ. Geol. Geophys.* 42, 1471–1475.
- Seltmann, R., Konopelko, D., Biske, G., Divaev, F., Sergeev, S., 2011. Hercynian post-collisional magmatism in the context of Palaeozoic magmatic evolution of the Tien Shan orogenic belt. *J. Asian Earth Sci.* 42, 821–838, <http://dx.doi.org/10.1016/j.jseas.2010.08.016>
- Simonov, V.A., Sakiev, K.S., Volkova, N.I., Stupakov, S.I., Travin, A.V., 2008. Conditions of formation of the Atbashi Ridge eclogites (South Tien Shan). *Russ. Geol. Geophys.* 49, 803–815, <http://dx.doi.org/10.1016/j.rgg.2008.04.001>
- Smye, A.J., Bickle, M.J., Holland, T.J.B., Parrish, R.R., Condon, D.J., 2011. Rapid formation and exhumation of the youngest Alpine eclogites: thermal conundrum to Barrovian metamorphism. *Earth Planet. Sci. Lett.* 306, 193–204.
- Su, W., Gao, J., Klemd, R., Li, J.-L., Zhang, X., Li, X.-H., Chen, N.-S., Zhang, L., 2010. U-Pb zircon geochronology of Tianshan eclogites in NW China: implication for the collision between the Yili and Tarim blocks of the southwestern Altaiids. *Eur. J. Mineral.*, <http://dx.doi.org/10.1127/0935-1221/2010/0022-2040>
- Sun, S., McDonough, W.F., 1989. In: Saunders, A.D., Norry, M.J. (Eds.), *Magmatism in the Ocean Basins*, vol. 42. Geological Society, London, pp. 313–345, Geological Society of London Special Publication.
- Suvorov, A.I., 1968. *Structure and Formation of Deep-Seated Faults* (in Russian). Trans. Geological Institute Academy of Sciences of the USSR, Moscow.
- Stacey, J.S., Kramers, J.D., 1975. Approximation of terrestrial lead isotope evolution by a two-stage model. *Earth Planet. Sci. Lett.* 26, 207–221.
- Tagiri, M., Yano, T., Bakirov, A.A., Nakajima, T., Uchiumi, S., 1995. Mineral paragenesis and metamorphic $P-T$ paths of ultra-high pressure eclogites from Kyrgyzstan Tien-Shan. *Isl. Arc* 4, 280–292.
- Tera, F., Wasserburg, G.J., 1972. U-Th-Pb systematics in three Apollo 14 basalts and the problem of initial Pb in lunar rocks. *Earth Planet. Sci. Lett.* 14, 281–304, [http://dx.doi.org/10.1016/0012-821X\(72\)90128-8](http://dx.doi.org/10.1016/0012-821X(72)90128-8)
- Tian, Z.L., Wei, C.J., 2013. Metamorphism of ultrahigh-pressure eclogites from the Kebuerte Valley, South Tianshan, NW China: phase equilibria and $P-T$ path. *J. Metamorph. Geol.* 31, 281–300, <http://dx.doi.org/10.1111/jmg.12021>
- Turbin, L.I., 1962. On the lower paleozoic stratigraphy of the western central Tien Shan. *Tr. Upr. Geol. i okhrany nedr pri SM KirgSSR*, 20–35.
- Tursungaziev, B.T., Petrov, O.V., 2008. *Geological Map of Kirghyz republic, Scale 1:500000* (in Russian). Saint-petersbg, VSEGEI.
- Von Raumer, J., Stampfli, G., Borel, G., Bussy, F., 2002. Organization of pre-Variscan basement areas at the north-Gondwanan margin. *Int. J. Earth Sci.* 91, 35–52, <http://dx.doi.org/10.1007/s005310100200>
- Von Raumer, J.F., Stampfli, G.M., 2008. The birth of the Rheic Ocean – early Palaeozoic subsidence patterns and subsequent tectonic plate scenarios. *Tectonophysics* 461, 9–20, <http://dx.doi.org/10.1016/j.tecto.2008.04.012>
- Von Raumer, J.F., Stampfli, G.M., Bussy, F., 2003. Gondwana-derived microcontinents – the constituents of the Variscan and Alpine collisional orogens. *Tectonophysics* 365, 7–22, [http://dx.doi.org/10.1016/S0040-1951\(03\)00015-5](http://dx.doi.org/10.1016/S0040-1951(03)00015-5)
- Wang, B., Faure, M., Shu, L., Cluzel, D., Charvet, J., De Jong, K., Chen, Y., 2008. Paleozoic tectonic evolution of the Yili Block, western Chinese Tianshan. *Bull. Soc. Geol. Fr.* 179, 483–490, <http://dx.doi.org/10.2113/gssgbull.179.5.483>
- Wang, B., Cluzel, D., Shu, L., Faure, M., Charvet, J., Chen, Y., Meffre, S., Jong, K., 2009. Evolution of calc-alkaline to alkaline magmatism through Carboniferous convergence to Permian transcurrent tectonics, western Chinese Tianshan. *Int. J. Earth Sci.* 98, 1275–1298, <http://dx.doi.org/10.1007/s00531-008-0408-y>
- Wang, B., Faure, M., Shu, L., de Jong, K., Charvet, J., Cluzel, D., Jahn, B., Chen, Y., Ruffet, G., 2010. Structural and geochronological study of high-pressure metamorphic rocks in the kekeshu section (Northwestern China): implications for the late paleozoic tectonics of the Southern Tianshan. *J. Geol.* 118, 59–77, <http://dx.doi.org/10.1086/648531>
- Warren, C.J., Waters, D.J., 2006. Oxidized eclogites and garnet-blueschists from Oman: $P-T$ path modelling in the NCFMASHO system. *J. Metamorph. Geol.* 24, 783–802.
- Waters, D., 2002. Clinopyroxene-amphibole-plagioclase symplectites in Norwegian eclogites: Microstructures, chemistry and the exhumation $P-T$ path. In: Mineralogical Society, Winter Conference, "Timing, Transition, and Tectonics". Derby University, UK (abstract).
- Waters, D., 2003. $P-T$ path from Cpx-Hbl-Pl symplectites, updated 22.02.03. <http://www.earth.ox.ac.uk/~davewa/research/eclogites/symplectites.html>
- Whitney, D.L., Evans, B.W., 2010. Abbreviations for names of rock-forming minerals. *Am. Mineral.* 95, 185–187, <http://dx.doi.org/10.2138/am.2010.3371>
- Wiedenbeck, M., Hanchar, J.M., Peck, W.H., Sylvester, P., Valley, J., Whitehouse, M., Kronz, A., Morishita, Y., Nasdala, L., Fiebig, J., Franchi, I., Girard, J.-P., Greenwood, R.C., Hinton, R., Kita, N., Mason, P.R.D., Norman, M., Ogasawara, M., Piccoli, P.M., Rhede, D., Satoh, H., Schulz-Dobrick, B., Skár, O., Spicuzza, M., Terada, K., Tindle, A., Togashi, S., Vennemann, T., Xie, Q., Zheng, Y.-F., 2004. Further Characterisation of the 91500 Zircon Crystal. *Geostand. Geanal. Res.* 28, 9–39.
- Windley, B.F., Alexeev, D.V., Xiao, V., Kröner, W.W., Badarch, A., Kröner, G.A., 2007. Tectonic models for accretion of the Central Asian Orogenic Belt. *J. Geol. Soc. London* 164, 31–47.
- Windley, B.F., Allen, M.B., Zhang, C., Zhao, Z.-Y., Wang, G.-R., 1990. Paleozoic accretion and Cenozoic reformation of the Chinese Tien Shan Range, Central Asia. *Geology* 18, 128, [http://dx.doi.org/10.1130-0091-7613\(1990\)018<0128:PAACRO>2.3.CO;2](http://dx.doi.org/10.1130-0091-7613(1990)018<0128:PAACRO>2.3.CO;2)
- Xiao, W., Windley, B.F., Allen, M.B., Han, C., 2013. Paleozoic multiple accretionary and collisional tectonics of the Chinese Tianshan orogenic collage. *Gondwana Res.* 23, 1316–1341, <http://dx.doi.org/10.1016/j.gr.2012.01.012>
- Xiao, X.C., Tang, Y.Q., Feng, Y.M., Zhu, B.Q., Li, J.Y., Zhao, M., 1992. *Tectonic Evolution of the Northern Xinjiang and its Adjacent Regions* (in Chinese with English Abstract). Geology Publishing House, Beijing.
- Yamato, P., Burov, E., Agard, P., Pourhiet, L., Le Jolivet, L., 2008. HP-UHP exhumation during slow continental subduction: self-consistent thermodynamically and thermomechanically coupled model with application to the Western Alps. *Earth Planet. Sci. Lett.* 271, 63–74, <http://dx.doi.org/10.1016/j.epsl.2008.03.049>
- Zhang, L.F., Du, J.X., Shen, X.J., Lü, Z., Song, S.G., Wei, C.J., 2009. The timing of UHP-HP eclogitic rocks in Western Tianshan, NW China: the new SIMS U-Pb zircon dating, Lu/Hf and Sm/Nd isochron ages. In: 8th International Eclogite Conference.